CHAPTER 5

CASE STUDY OF THE FORT ST. JOHN GRABEN AREA

The deltaic sandstones of the basal Kiskatinaw Formation (Stoddart Group, upper Mississippian) were preferentially deposited within structural lows in a regime characterized by faulting and structural subsidence. In the case study of the Fort St. John Graben area, northwest Alberta, Canada, these sandstone facies can form reservoirs where they are laterally sealed against the flanks of upthrown fault blocks. Exploration for basal Kiskatinaw reservoirs generally is accompanied by the acquisition and interpretation of surface seismic data prior to drilling. These data are used to map the grabens in which these sandstones were deposited, and the location of horst blocks which act as lateral seals. Subsequent to drilling, three vertical seismic profile (VSP) surveys were conducted at the 9-24-82-11 W6M exploratory well site. These data supplemented the surface seismic and well log control such that (Hinds et al., 1991a; Hinds et al., 1993a; Hinds et al., 1994c):

1) direct correlation is made with the surface seismic data. As a result, the surface seismic control was accurately tied to the subsurface geology and geological seismic markers;

2) multiples were positively identified on the VSP data and the effect of these events on the surface seismic interpretation was determined; and

3) the subsurface geology, in the vicinity of the borehole, is more clearly resolved on the

VSP data than on the surface seismic control and an investigation of the basal Kiskatinaw revealed amplitude anomalies and local faulting which was not evident on the surface seismic data (Hinds et al., 1994b).

This chapter is a case history of the Fort St. John Graben 9-24 well (as reported in Hinds et al., 1991a; Hinds et al., 1993a and 1994b). An overview of the stratigraphy (Fig. 5.1) and the geologic history of the Lower Carboniferous in the study area is included. The acquisition and interpretive processing of the VSP data is described, and an integrated interpretation of the well log, surface seismic and seismic profile data is presented.

On the Fort St. John Graben dataset described in this chapter, faults which are not well resolved on the surface seismic data are better delineated on the VSP data. The interpretive processing of these data illustrate the utility of the seismic profiling technique to the search for hydrocarbons in structurally complex areas.

5.1 Introduction

On the basis of conventional surface seismic data, an exploratory well (9-24-82-11 W6M) was drilled into the basal Kiskatinaw Formation (Stoddart Group, upper Mississippian; Fig. 5.1) on the downthrown side of a fault block in the Fort St. John Graben area, Peace River Embayment (Fig. 5.2 and 5.3). It was expected that gas-prone sandstones of the basal Kiskatinaw would be laterally truncated and sealed against shales of the Golata Formation. Contrary to expectations, the well encountered unproductive, shaly sandstone tidal-flat facies

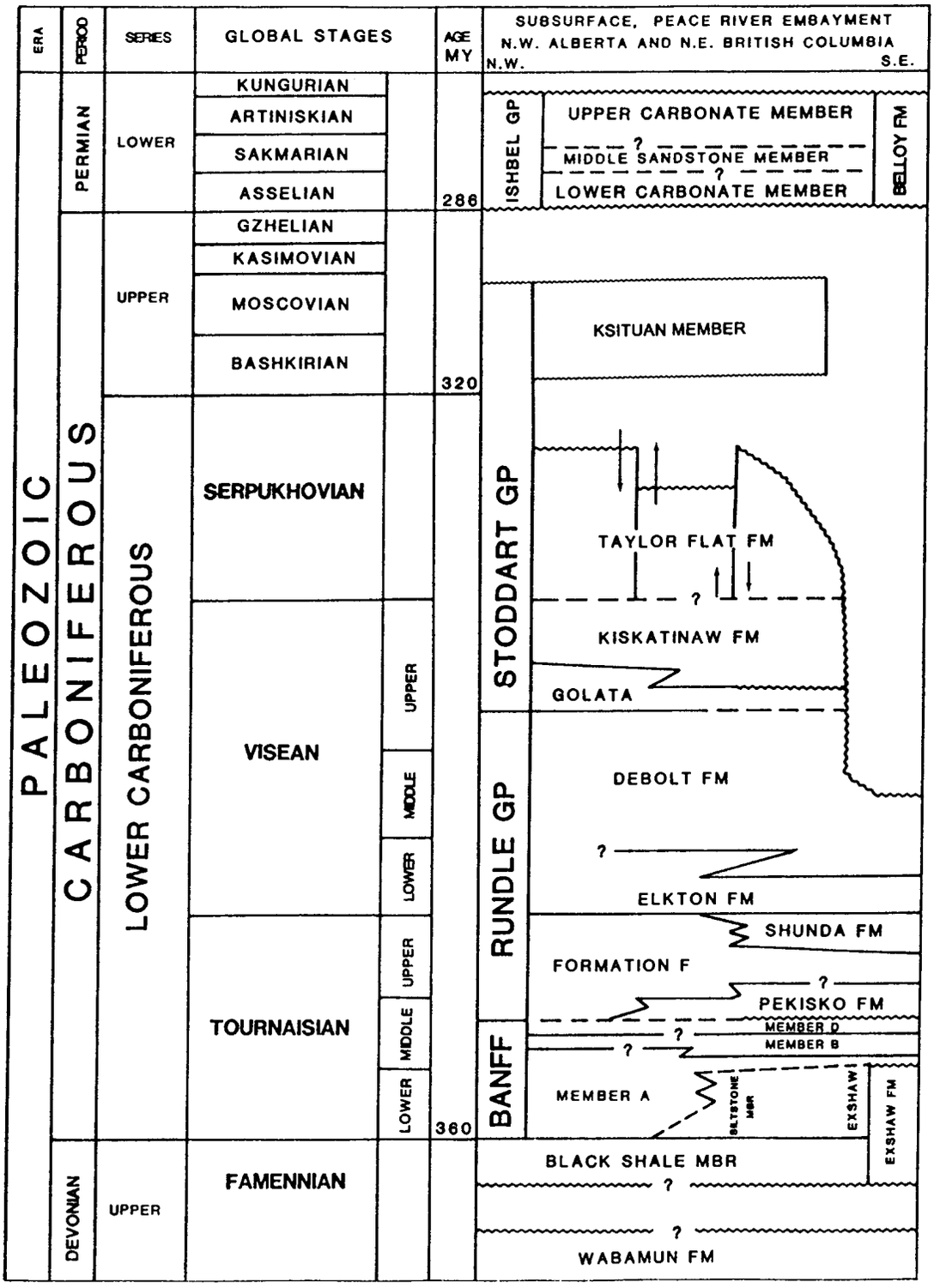

Figure 5.1 Stratigraphy of the Fort St. John Graben study area (modified from Richards, 1989).

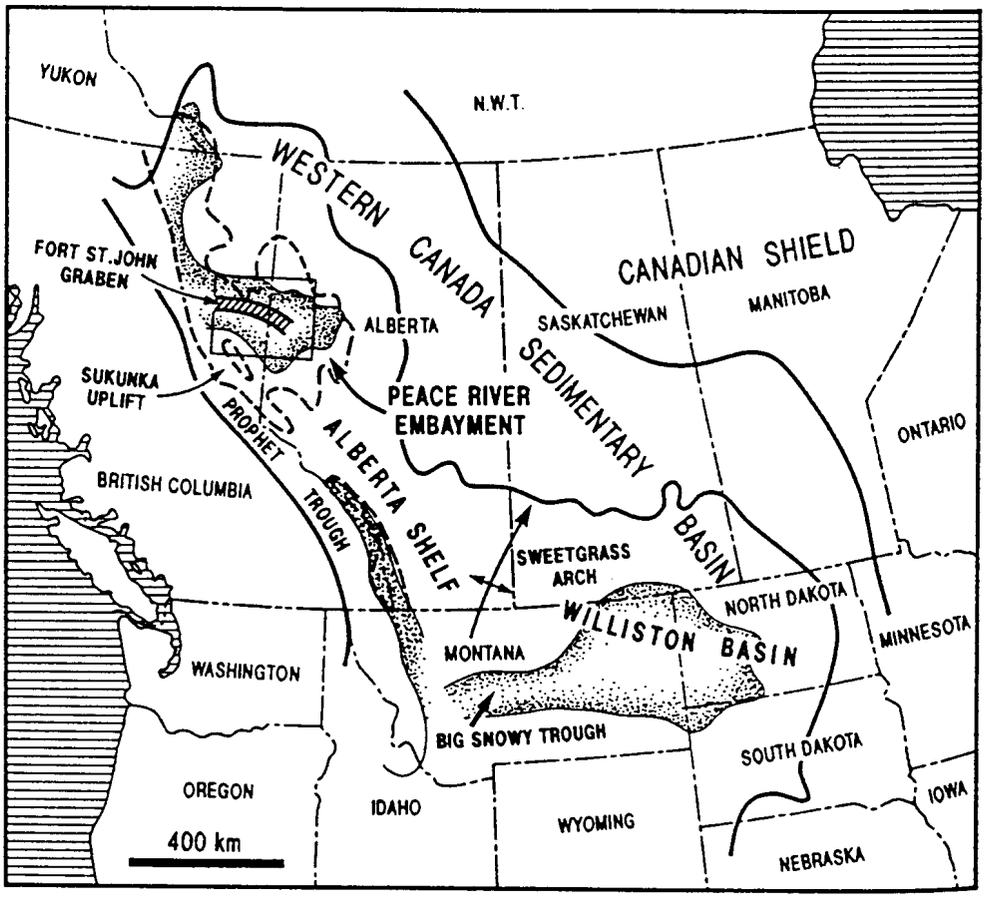

Figure 5.2 Map of Western Canadian Sedimentary Basin tectonic elements showing the Peace River Embayment, Prophet Trough, Sukunka Uplift, cratonic platform and Fort St. John Graben. (Barclay et al., 1990)

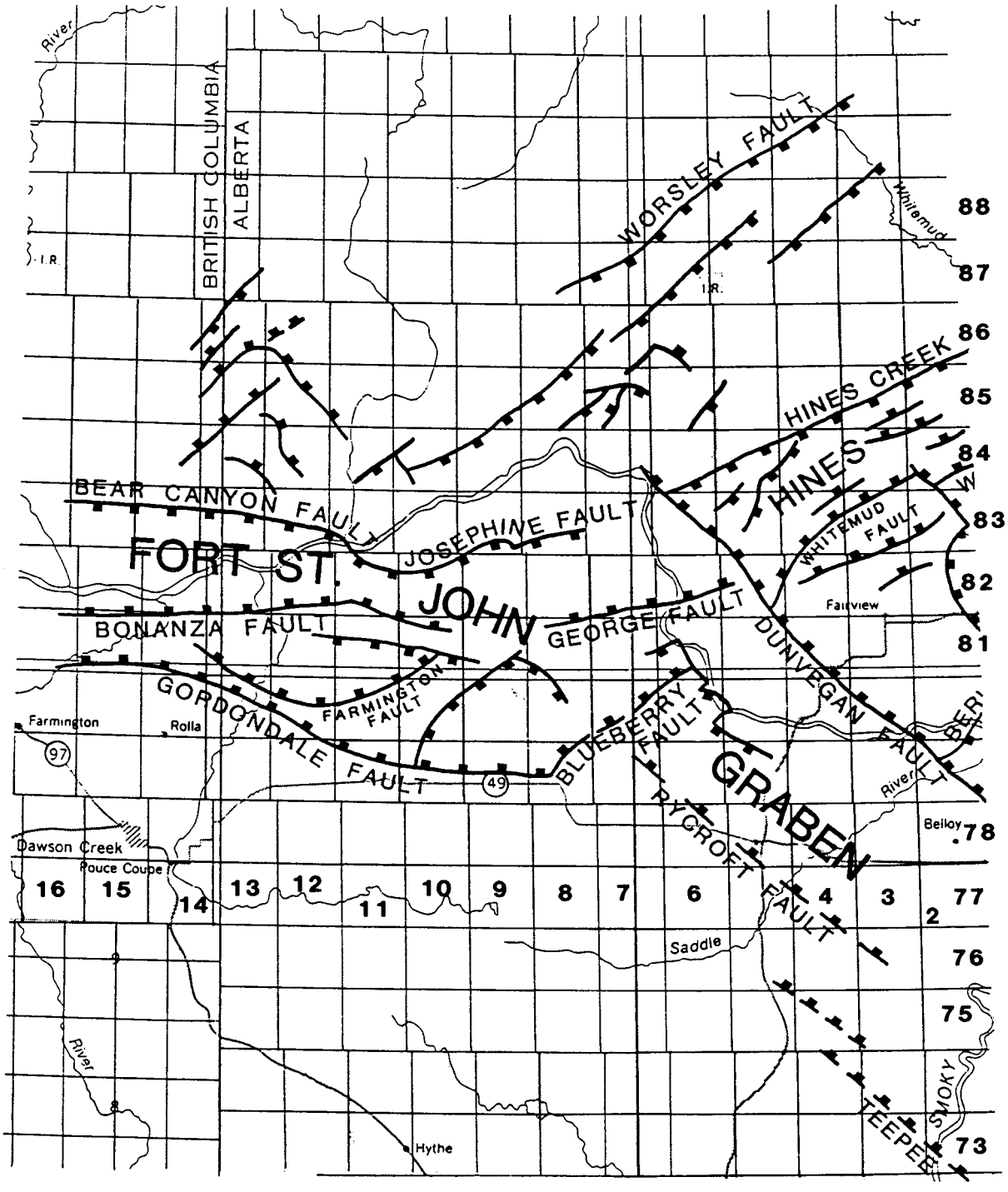

Figure 5.3 Detailed area map of the Fort St. John Graben showing the Bear Canyon, Josephine, Bonanza and George faults (from Richards et al., 1994). The study area is centred in Township 82 and Range 11 west of the 6th Meridian in Alberta, Canada near the Alberta and British Columbia provincial border.

in the basal Kiskatinaw and a commercial gas-bearing zone in the upper Kiskatinaw, and is now shut-in (Hinds et al., 1991a; Hinds et al., 1993a and 1994b).

To obtain a higher resolution image of the subsurface in the vicinity of well 9-24, and to evaluate the presence and proximity of any fault features which might not have been resolved on the surface seismic data, three VSP (vertical seismic profile) surveys were designed and performed at the 9-24 well site. These profiles were used in conjunction with surface seismic coverage to cooperatively image the fault systems in the area and to elucidate the seismic signature of the upper Kiskatinaw reservoir which had not been prognosed.

5.2 Geological overview

5.2.1 Tectonic and depositional history of the Peace River Embayment

This section will review the tectonic and depositional history for the study area. Unlike the case studies of chapters 3, 4, and 6 which pertain to carbonate reef exploration in the WCSB; this case study pertains to channel sand deposition and hydrocarbon entrapment within. The following section will review the stratigraphy of the study area.

Investigation of the Peace River Arch and Peace River Embayment revealed a depositional regime characterized by faulting (O'Connell, 1990) and structural subsidence. The Peace River Arch can be traced to a crustal structure consisting of uplifted granitic basement (Fig. 5.4a; Cant , 1988) and subsequently was deformed in three main phases:

1) the formation of a structural high in the latest Late Proterozoic which was onlapped by siliciclastic, evaporite and carbonate deposition until the Middle to Late Devonian;

The basement was uplifted 800 to 1000 m above the regional elevation (Cant, 1988) during the early Paleozoic (mid-Cambrian) as an asymmetrical feature with the northern flank dipping steeply and the southern flank dipping more gently (O'Connell et al., 1990). During the Middle to Upper Devonian, a diachronous siliciclastic unit (lithozone as defined in Trotter, 1989) called the Granite Wash (sediments derived from plutonic and metamorphic basement relics) and carbonate and shale deposits of the Elk Point (along with Gilwood sandstone), Beaverhill Lake (Slave Point, carbonate reefs and Waterways Fm) , Woodbend (fringing reefs, basal ramp to stacks of carbonate shelves and overlying carbonate ramp) and Winterburn (Nisku and Blueridge Fm; Moore, 1988) Groups onlapped onto the emergent arch. The Wabamun Fm carbonates eventually buried most of the Arch. Another feature existing during the deposition of the Wabamun Fm was localized islands of subaerially exposed Granite Wash Fm that were present during the deposition of the lower Banff Fm (Richards, 1991, pers. comm.).

2) the formation of a series of embayments resulting in anomalously thick Carboniferous, Permian and Triassic deposits;

During the deposition of the Middle Devonian Elk Point Group, normal faulting began. These normal faults were rejuvenated in the late Famennian during the deposition of the upper Wabamun Fm and the overlying Exshaw Fm (Fig. 5.4b).

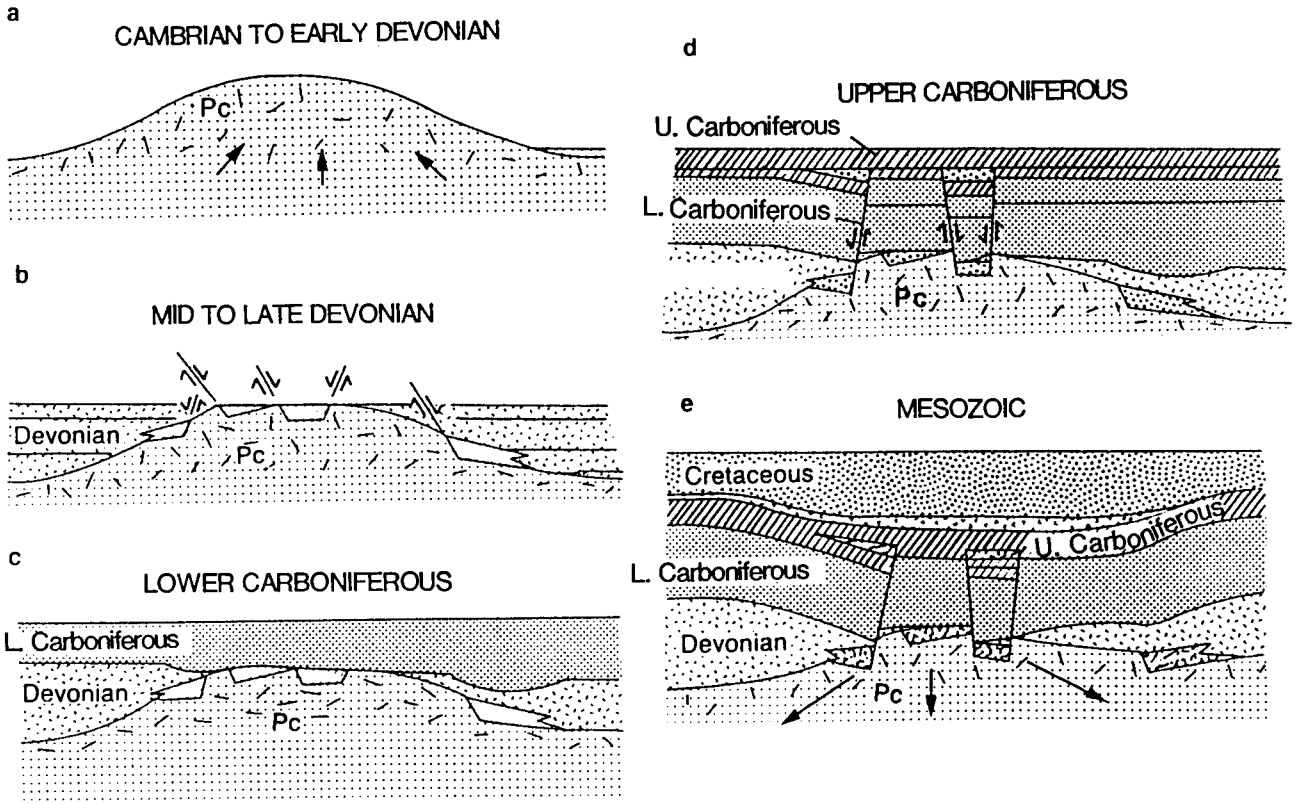

Figure 5.4 Diagrammatic summary of the depositional and tectonic history of the Peace River Embayment area (from Cant, 1988) from the Cambrian to the Cretaceous periods.

3) the development of a deep basin component of the foreland basin during the Jurassic and Cretaceous.

The arch ceased to be emergent by the beginning of the Carboniferous.

The Peace River Embayment, a structural inversion consisting of northeast to southwest trending interlinked graben and half-grabens (Barclay et al., 1990), started to develop during the latest Devonian (late Famennian) and earliest Carboniferous when the Exshaw and overlying lower Banff Fm were deposited (Richards, 1989; Richards et al., 1994). The major tectonic features surrounding the Embayment were the Prophet Trough (Richards, 1989; Richards et al., 1994), Sukunka Uplift (Richards, 1989) and cratonic platform (Fig. 5.2). The northwest-trending narrow pericratonic Prophet Trough (O'Connell et al., 1990) resulted from the downwarping and downfaulting of the western margin of the North American plate during the latest Devonian (late Famennian) and Carboniferous and is interpreted as a back-arc basin (Richards, 1989). In the detailed stratigraphic correlation chart (Fig. 5.1), the Famennian to Tournaisian boundary coincides with the Devonian to Carboniferous boundary. The Carboniferous Peace River Embayment opened northwestward into the Prophet Trough. During the middle to late Tournaisian, the Embayment became better defined as a separate entity. The northern Sukunka uplift on the southwestern side of the Embayment formed a low rim that restricted the access of the Embayment sediments into the southeastern part of the Prophet Trough.

Regional subsidence continued associated with extensive block faulting (Fig. 5.4d) along normal faults (Cant, 1988). During the period of block faulting, anomalously thick Lower

Carboniferous successions of siliciclastics and ramp-to-platform carbonates were deposited along the axis of the embayment (Richards, 1989, 1990).

The Devonian and Carboniferous tectonic history of the Peace River Embayment has been summarized by Richards (1989, 1990) and Richards et al. (1994). The onset of its development is postulated to be the late Famennian to early middle Tournaisian. During that initial time, the deposition of the Exshaw Fm and the overlying lower Banff Fm occurred (Richards, 1990).

5.2.2 Lower Carboniferous: Fort St. John Graben Area

Within the Carboniferous succession in the Fort St. John Graben study area (Fig. 5.3), four principal episodes of blockfaulting have been recognized (Richards 1989, 1990):

1) after deposition of the latest Devonian to earliest Carboniferous deposits of the Exshaw Fm but prior to the deposition of the overlying Banff Fm;

2) during deposition of the lower Banff Fm (early middle Tournaisian);

3) during the deposition of the Golata and Kiskatinaw Formations (late Visean); and

4) after deposition of the upper Visean to Serpukhovian (?) Taylor Flat Fm but prior to that of the Permian Ishbel Group.

Marked regional subsidence accompanied the second and third phases of blockfaulting, whereas subaerial erosion and local uplift accompanied the first and last phases. Pronounced regional subsidence, at least locally, accompanied by blockfaulting also took place during deposition of the middle and upper Tournaisian Pekisko and Shunda Formations. In the middle Tournaisian, the developed embayment can best be termed a deep re-entrant into the western cratonic platform and the Prophet Trough is interpreted as a back arc basin (Richards, 1989). Deep-water environments existed in the embayment area during periods of pronounced subsidence. In the general study area, the Fort St. John and Hines Creek Grabens (Barclay et al., 1990) were already developing before the deposition of the Stoddart Group.

The Lower Carboniferous deposition spans from the upper part of the Exshaw Fm to the top of the Taylor Flat Fm. Carbonate and fine-grained terrigenous clastics were deposited during the Exshaw-Debolt interval. Basal shale, carbonate ramp deposits, shallow water shelf carbonates, inter- to supratidal carbonate, clastics and evaporites were deposited in the Banff Fm. Shales are also found in the Pekisko Fm, a coeval correlative for the Pekisko and Shunda defined in Richards (1989) called Formation F and Shunda Fm which overlie the Banff Fm. A well developed basin, slope and shelf environment in the Peace River Embayment was developed during the deposition of the lower and middle Banff Fm and during the Pekisko/Shunda succession. Apart from these times, sedimentation in the area kept pace with the subsidence which resulted in normal topographic relief.

The Golata, Kiskatinaw and Taylor Flat Formations were deposited in the late Visean and Serpukhovian subsequent to the deposition of the Debolt Fm with the Golata overlying the

Debolt Fm conformably in the central part of the embayment. The Golata consists of fissile grey mudstone, siltstone and shale (Barclay, 1988). Towards the basin margins, the Golata and Debolt contact becomes disconformable (O'Connell et al., 1990).

The Kiskatinaw consists predominately of sandstone with minor quantities of fine grained siliciclastics, limestones, dolostones and coals. At least eight depositional cycles make up the formation, but three main depositional cycles are referred to informally as the lower, middle and upper Kiskatinaw. The Kiskatinaw Fm represents a marine-dominated deltaic system which may have resembled an estuary in the study area during deposition (Richards, 1989; Richards et al., 1994). The study area was a semi-enclosed body of coastal water. Blockfaulting occurred accompanied by deep subaerial erosion which resulted in substantial thickness changes in the Kiskatinaw and Taylor Flat Fm deposits.

The Kiskatinaw and Golata Fm contact is unconformable. This prodelta sequence (Golata Fm) can serve as a reservoir seal in those places where, as a result of faulting, it is juxtaposed against the sandstones of the basal Kiskatinaw. The uppermost and basal Kiskatinaw Fm sandstones deposits are exploration targets.

The deposition in the study area is shown in the models for the Stoddart Group deposition in figure 5.5a-d (from Barclay et al., 1990; Fig. 17a-d). The creation of the hydrocarbon trapping structures occurred prior to the deposition of the Permian Belcourt and Belloy Fm.

The study area is in the Fort St. John Graben area defined by East-West faulting to the North

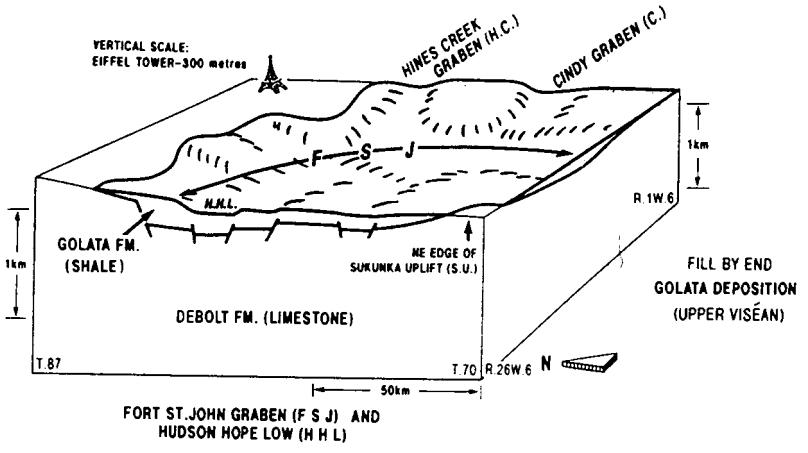

Figure 5.5A Block diagram showing the Fort St. John Graben deposition by the end of the Golata Formation time (from Barclay et al., 1990).

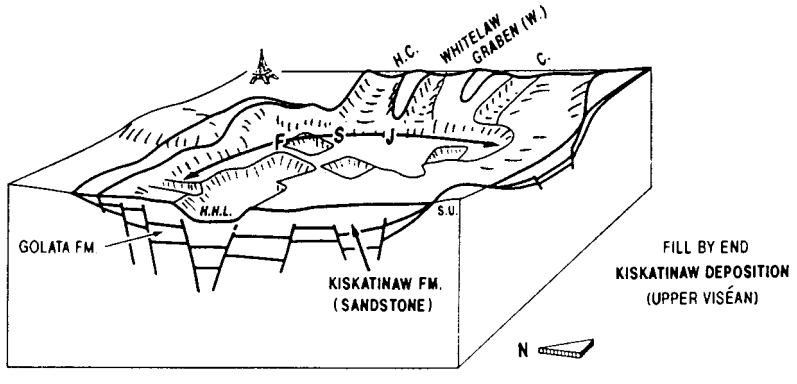

Figure 5.5B Block diagram showing the Fort St. John Graben deposition by the end of the Kiskatinaw Formation time (from Barclay et al., 1990).

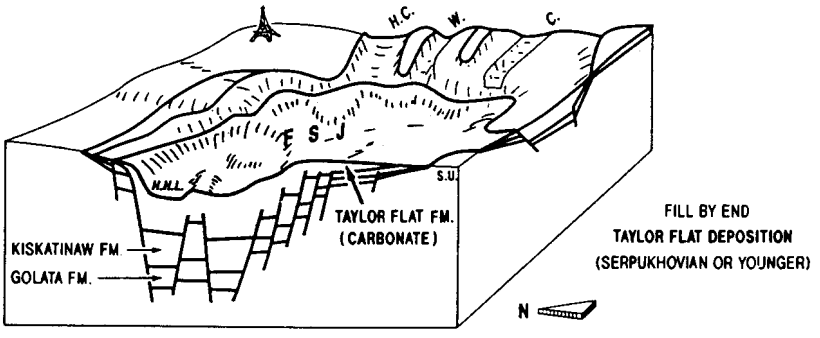

Figure 5.5C Block diagram showing the Fort St. John Graben deposition by the end of the Taylor Flat Formation time (from Barclay et al., 1990).

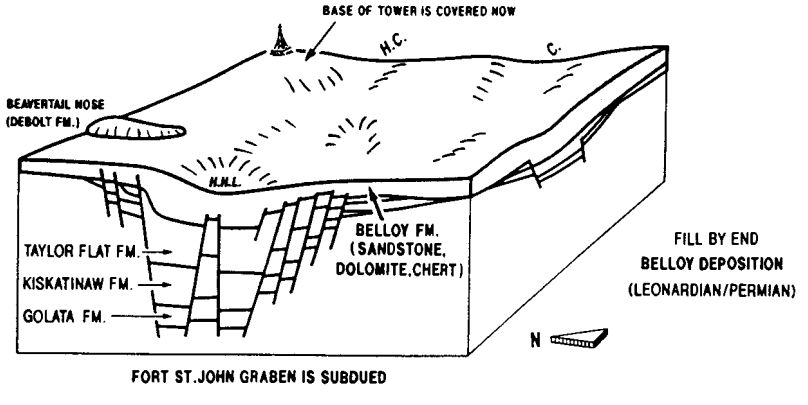

Figure 5.5D Block diagram showing the Fort St. John Graben deposition by the end of the Belloy Formation time (from Barclay et al., 1990).

(Bear Canyon and Josephine faults) and to the South (Bonanza fault) as shown in Figure 5.3. The Fort St. John Graben is part of the Dawson Creek Graben Complex (Barclay et al., 1990) as is shown in figure 5.6 and 5.7.

The channel fill making up the basal Kiskatinaw (Barclay, 1988) were the target of the 9-24 well. The hypothesis was that thick sections of basal Kiskatinaw would be preferentially deposited in the structural lows on the downthrown side of early Kiskatinaw faults. The basal Kiskatinaw encountered by the 9-24 well was not of reservoir quality; however, the sandstones of the upper Kiskatinaw contain commercial gas.

5.3 Original interpretation and well results

Seismic data interpreted by the owners of the well prior to the drilling of well 9-24 and the running of the VSP surveys are shown in Figure 5.8. All subsequent interpretation on data presented within this chapter are presented as part of the thesis research.

The split-spread, 96 pre-stack trace data used to create the stacked section (Fig. 5.8) were acquired using a patterned dynamite source (3 X 3 kg at 15 m) and DFS4 recording equipment (12/18-124 Hz filter; notch (60 Hz) filter out). The groups consisted of nine inline 14-Hz L25D geophones spaced at 6.1 m. The geophone group, shot, common mid-point (CMP), and near offset intervals were 67.1, 134.1, 33.5, and 201.2 m respectively.

The seismic section (normal polarity display; Fig. 5.8) was migrated using a prestack partial

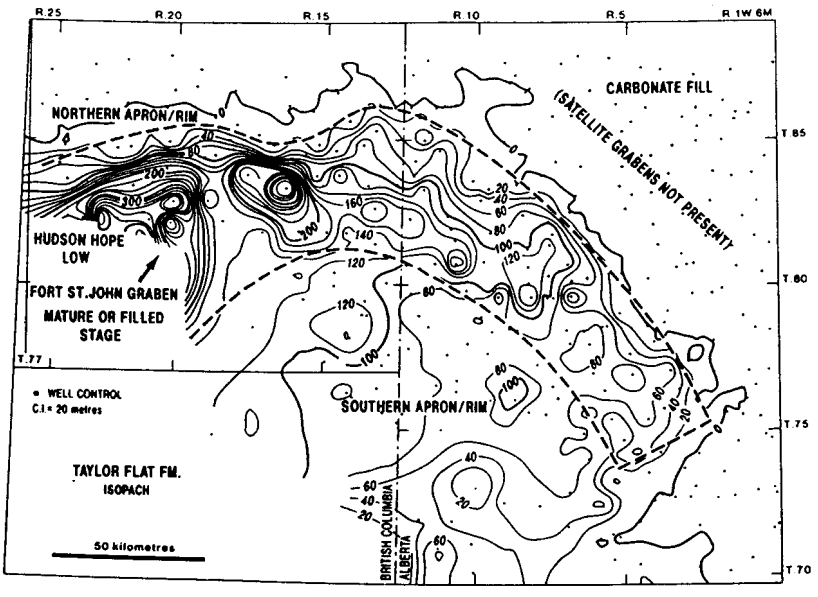

Figure 5.6 Location of the Fort St. John Graben as outlined by the Belloy Formation isopach map (from Barclay et al., 1990). The Belloy deposition marked the end of the subsidence in the graben.

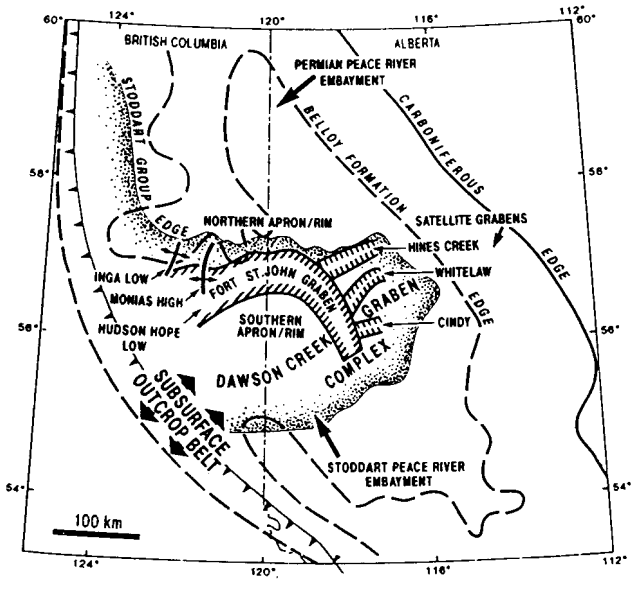

Figure 5.7 Peace River Embayment stratotectonic elements including the Fort St. John Graben (from Barclay et al., 1990).

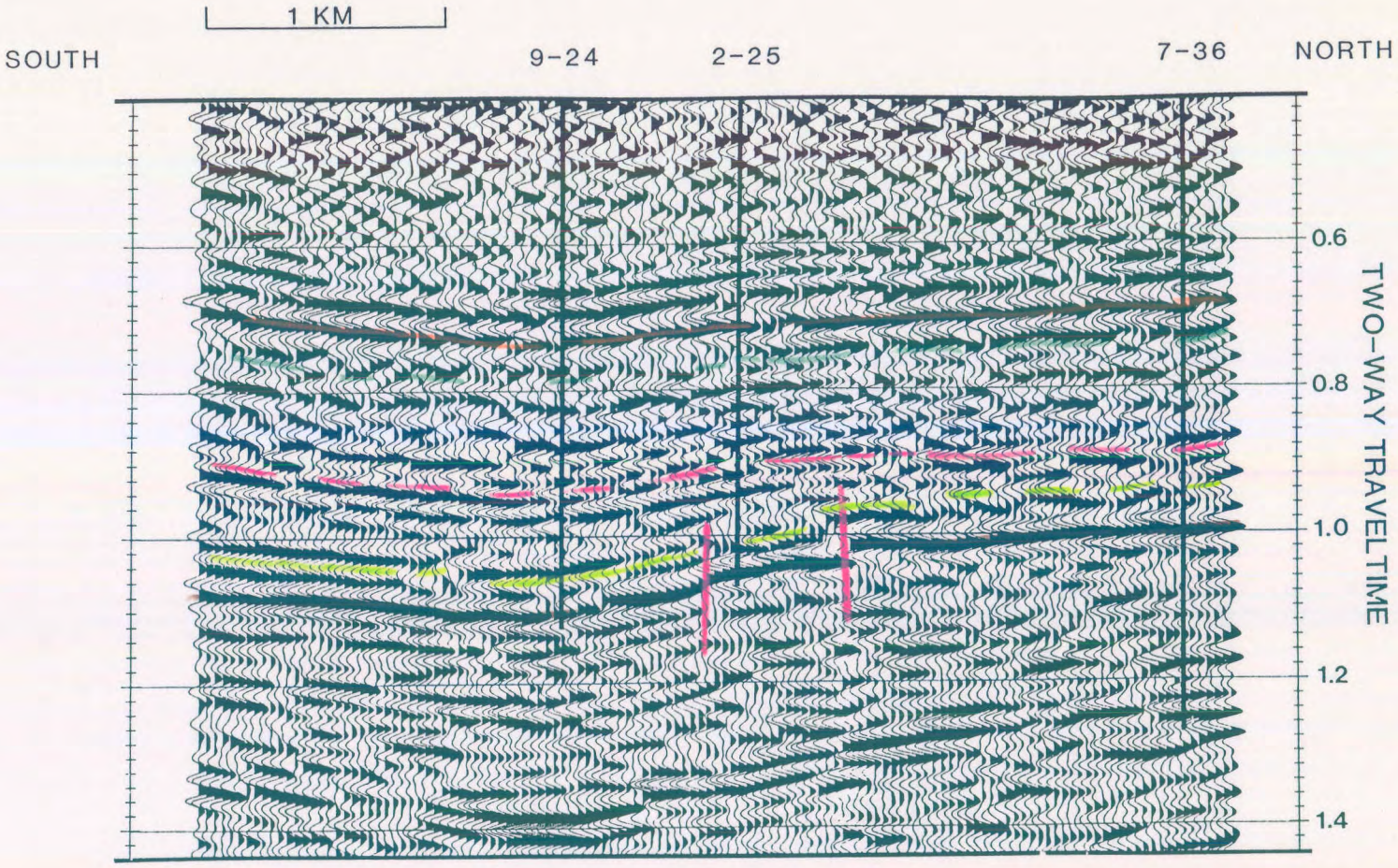

Figure 5.8 Example surface seismic data displaying the original interpretation of the owners of the 9-24 well (preceding the drilling of the well). The data suggested one major fault between the intended well 9-24 and the existing well 2-25.

migration scheme which consisted of applying a common-offset domain, dip-moveout (DMO) correction (Hale, 1984) to the prestack data. Updated velocities were then determined using the DMO-corrected CMP gathers. Closely spaced velocity analyses were performed since the stacking velocities changed rapidly along the line. This prestack processing was followed by poststack phase-shift migration. The poststack migration method is reviewed in Gazdag (1978) and Gazdag and Squazzero (1984).

The surface seismic data were used to elucidate the structural setting at the Kiskatinaw level. The interpreted events on the seismic line are the Nordegg, Halfway/Doig, Belloy, basal Kiskatinaw, and Debolt (stratigraphically listed in Fig. 5.1). The 9-24-82-11 W6M well was located approximately 200 m east of the seismic line and has been projected onto the seismic line as shown in Figure 5.8. Note that 9-24, as projected, is on a downthrown fault block relative to 2-25-82-11 W6M and 7-36-82-11 W6M (Fig. 5.8).

Well 2-25 encountered approximately 25 m of relatively clean, wet basal Kiskatinaw sandstone and was abandoned. Well 7-36 penetrated 35 m of basal Kiskatinaw sandstone which tested gas plus salt water and is currently classified as a shut-in gas well. Well 9-24 was drilled in the expectation that basal Kiskatinaw gas would be stratigraphically entrapped against the flank of the upthrown flank block; however the basal Kiskatinaw proved to be shaly-sandstone and not of reservoir quality. 9-24 was shut-in as an upper Kiskatinaw gas well.

5.4 VSP acquisition

Three VSP surveys were run at the 9-24 well site (one near offset and two far offset sources). The VSP were planned with the following objectives in mind:

1) to provide a confident surface seismic tie to:
   a) the upper Kiskatinaw Fm reservoir;
   b) the lower Kiskatinaw Fm; and
   c) the Debolt Fm;

2) to determine if multiple reflections were a significant problem at the Kiskatinaw level, and to design an effective deconvolution filter;

3) to map the lateral extent of the shaly sandstone of the basal Kiskatinaw and upper Kiskatinaw reservoir in the direction of the far offset VSPs; and

4) to provide a higher resolution seismic image of the Debolt fault in the vicinity of the 9-24 well.

The near offset VSP source was located 149 m from well 9-24 and in the direction of well 2-25. One of the far offset source locations (referred to as FSJG1 in chapter 2) was in the direction of 2-25 and 700 m from the 9-24 well site. The other far offset source location (referred to as FSJG2) was situated 741 m east of well 9-24. Two Vibroseis units operated

in series at each offset using a 12 second sweep of 10-90 Hz. The recording length was 15 seconds resulting in a 3 s cross-correlated output. On average, six sweeps were summed at each geophone sonde location. The total depth of well 9-24 was 2126 m below Kelly Bushing of the drilling rig (KB at 644 m asl). All three offset sources were at 639 m asl. Data were recorded at a sampling rate of 1 ms using an MDS-10 unit. The recording filter, OUT/250, was designed to prevent aliasing.

The triaxial sonde vertical spacing was 20 m (from a depth of 2030 m up to 350 m). As a precautionary measure, calibration records were acquired at several depths as the sonde was lowered down the borehole and repeated again during the production runs to detect possible depth errors or cable stretch.

5.5 Near offset (149 m) VSP interpretive processing

During the processing of the near offset VSP data, a series of interpretive processing panels (IPPs) were designed. These panels were designed to display the following interpretive processing steps (Hinds et al. 1991a; Hinds et al., 1993a and 1994b; and Hinds et al., 1994c):

1) upgoing and downgoing P-wave separation;

2) deconvolution of the separated upgoing P-waves; and

3) inside and outside corridor stacks of both the nondeconvolved and deconvolved upgoing waves.

5.5.1 P-wave event separation

The separation of the upgoing and downgoing P-waves from the Z(FRT) data is displayed in the wavefield separation interpretive processing panel (Hinds et al., 1989a; Hinds et al., 1993a; Hinds et al., 1994c) of Figure 5.9.

Panel 1 displays the Z(FRT) data after trace normalization. The upgoing P-wave events are difficult to discern until the Z(FRT) data are gained (panel 2). On these panels, the tube wave is visible below 0.9 s as a high-frequency, downgoing wavetrain with a velocity of propagation of about 1435 m/s. The tube wave reflects from the bottom of the well borehole and travels back up. This accounts for the upgoing tubewave F-K events discussed in chapter 2.

Several upgoing primary events and multiple reflections can be identified on panel 2. Consider for examples, the Spirit River and Nordegg events which are highlighted in blue and orange, respectively. Each of these events is followed by a trailing surface-generated multiple with a lag time of about 110 ms. This multiple pattern (both upgoing and downgoing waves) is highlighted in panel 2 of Figure 5.9.

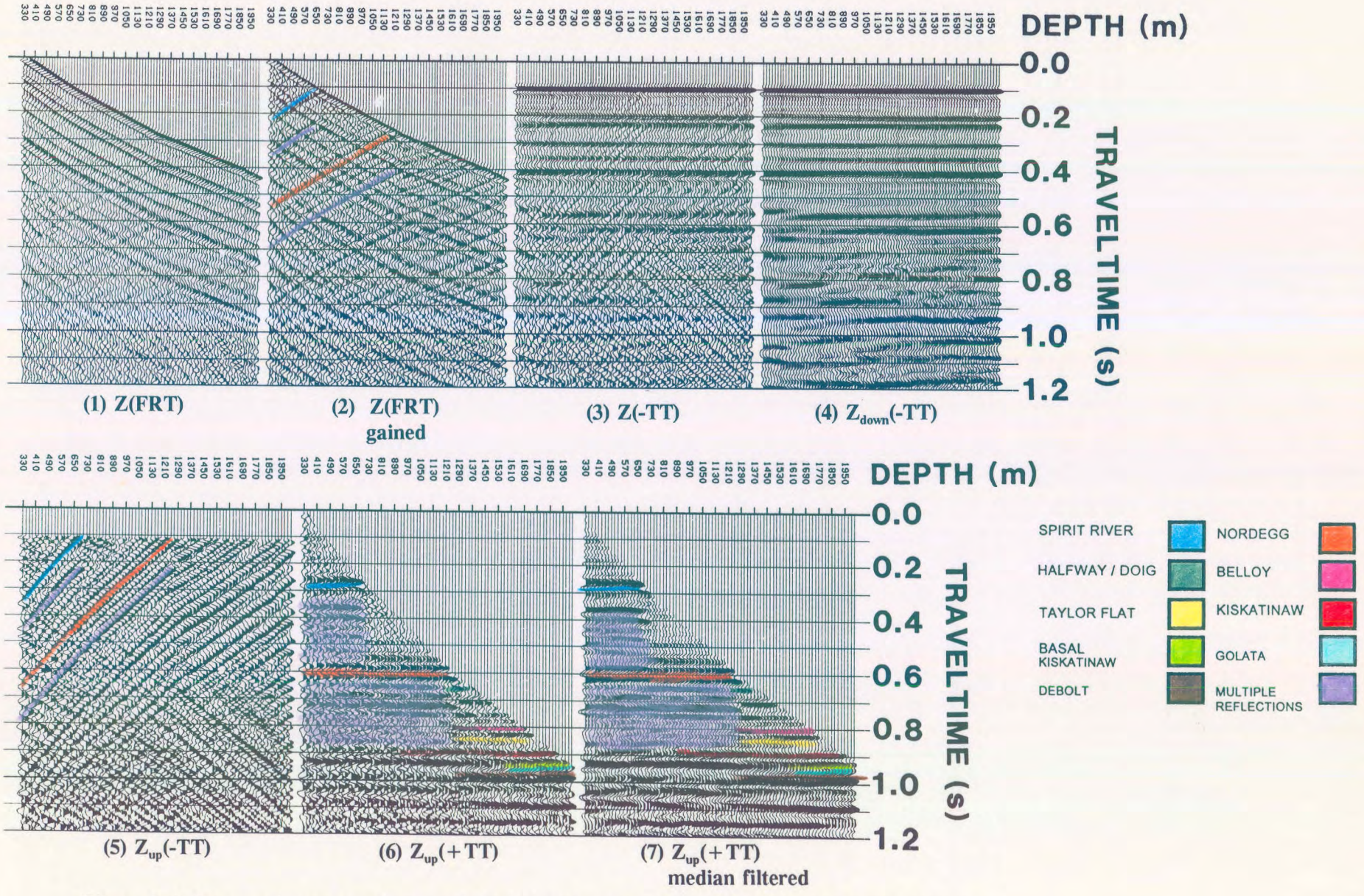

Figure 5.9 Interpretive processing panel depicting the wavefield separation of the near offset Fort St. John Graben VSP data (from Hinds et al., 1993a).

In panel 3 (Fig. 5.9), the **Z(-TT)** data are displayed. An 11-point median filter was used to remove the upgoing P-waves; the $\mathbf{Z_{down}(-TT)}$ data are displayed in panel 4. In the next step, the $\mathbf{Z_{down}(-TT)}$ data of panel 4 were subtracted from the **Z(-TT)** data to yield the $\mathbf{Z_{up}(-TT)}$ data (panel 5). Note that a residual tube wave is visible within the $\mathbf{Z_{up}(-TT)}$ data panel.

The $\mathbf{Z_{up}(+TT)}$ data before and after the application of a 3 point median filter are shown in panels 6 and 7, respectively. The two panels have been time shifted to facilitate plotting. In panel 7, the Spirit River multiple (highlighted in panel 2) is observed as high amplitude events which lie directly below the Spirit River primary and can be interpreted for several cycles (from 0.3 to 0.7 s). This multiple is not observed at sonde depths deeper than the top of the Spirit River (at 730 m).

5.5.2 Near offset VSP deconvolution

Deconvolution IPP (Hinds et al., 1989a) were designed for the $\mathbf{Z_{up}(+TT)}$ data (Fig. 5.10) to enable the monitoring of the deconvolution process for the near offset data (Hinds et al., 1993a; Hinds et al., 1994c). The incorporated panels reveal information (about multiples) that was difficult to determine from the wavefield separation IPP (Fig. 5.9) alone. The first two panels (Fig. 5.10) are the nonfiltered and median-filtered $\mathbf{Z_{up}(+TT)}$ data, respectively. The interpreted multiple events have been highlighted in purple on panels 1 and 2.

Panel 3 is the gained $\mathbf{Z_{down}(-TT)}$ data. Panels 4 and 5 are the nondeconvolved and deconvolved $\mathbf{Z_{up}(-TT)}$ data, respectively, which enable an evaluation of the effect that the deconvolution process has on the $\mathbf{Z_{up}(-TT)}$ data.

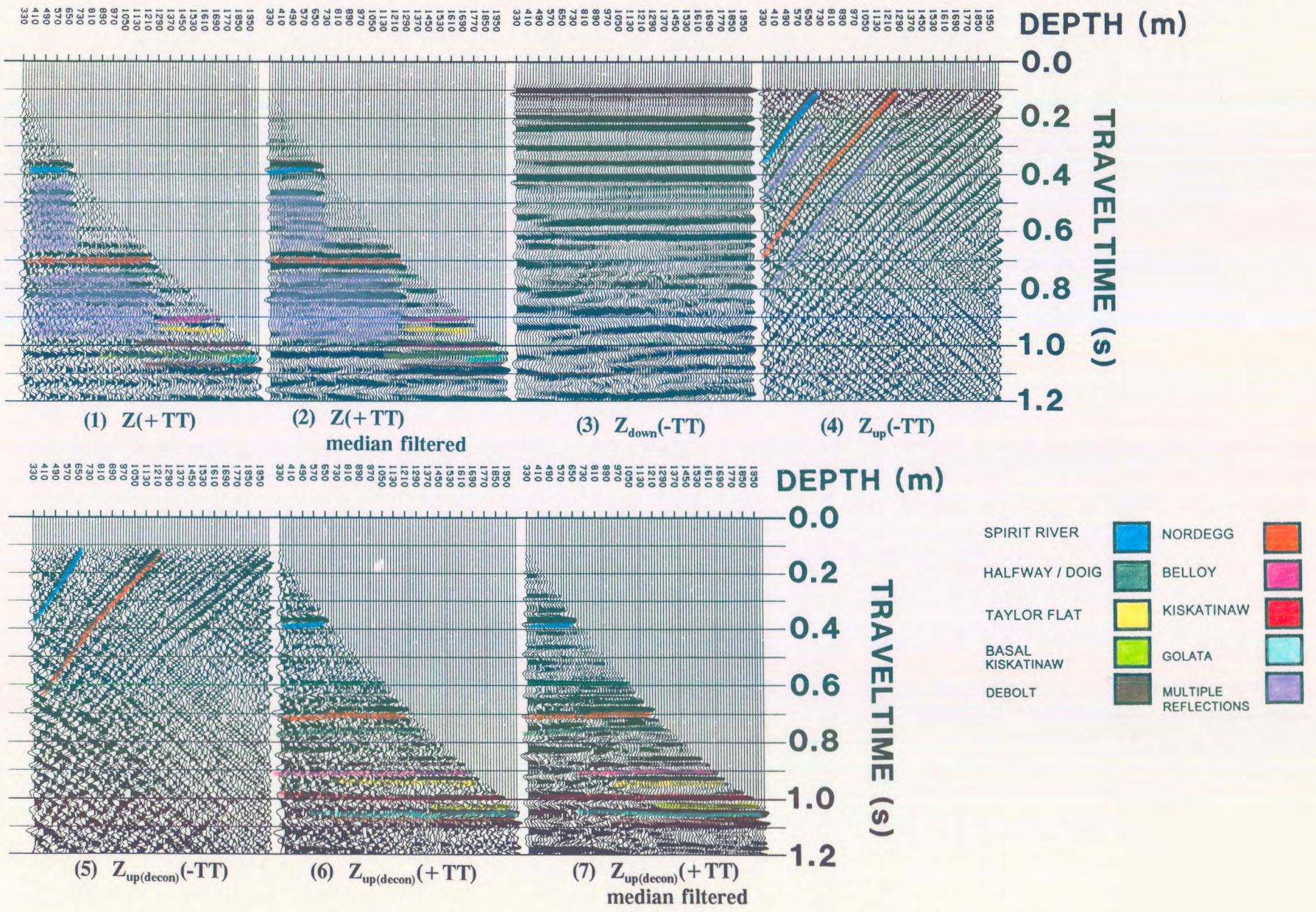

Figure 5.10 Interpretive processing panel depicting the deconvolution of the near offset Fort St. John Graben VSP data (from Hinds et al., 1993a).

The last two panels (6 and 7) are the nonmedian and median-filtered $\mathbf{Z_{up(decon)}(+TT)}$ data, respectively. By inspection of panels 2 and 7 (Fig. 5.10), it is interpreted that the deconvolution processing has effectively attenuated multiple reflections. The Spirit River multiple wavetrain from 0.5 to 0.9 s on panel 2, for example (coloured in purple), has negligible amplitude on panel 7. Note also that deconvolution has increased the frequency content of the data, allowing for better resolution at the Kiskatinaw level.

5.5.3 Inside and outside corridor stacks

Nondeconvolved, inside and outside corridor stacks and associated displays (Hinds et al., 1989a) were designed for the near offset data as presented in Figure 5.11 (Hinds et al., 1993a; Hinds et al. 1994c). A comparison of the inside and outside corridor stacks (panels 3 and 4, respectively) illustrates the utility of these displays. For example, the Spirit River multiple (between 0.65 and 1.0 s) is present on the inside corridor stack and absent on the outside corridor stack. Note also, that basal Kiskatinaw and Golata events can be resolved on the outside corridor stack; on the inside corridor stack these reflections are masked by a high-amplitude multiple.

If deconvolution is successful, the deconvolved inside and outside corridor stacks (panels 3 and 4; Fig. 5.12) should be similar . At the zone of interest just above 1.35 s, the Debolt and the Golata are similar (panels 3 and 4), however the basal Kiskatinaw is not adequately represented on the inside corridor stack of the deconvolved data. An examination of the input data to the inside corridor stack (panel 2 of Fig. 5.12) reveals that the multiple

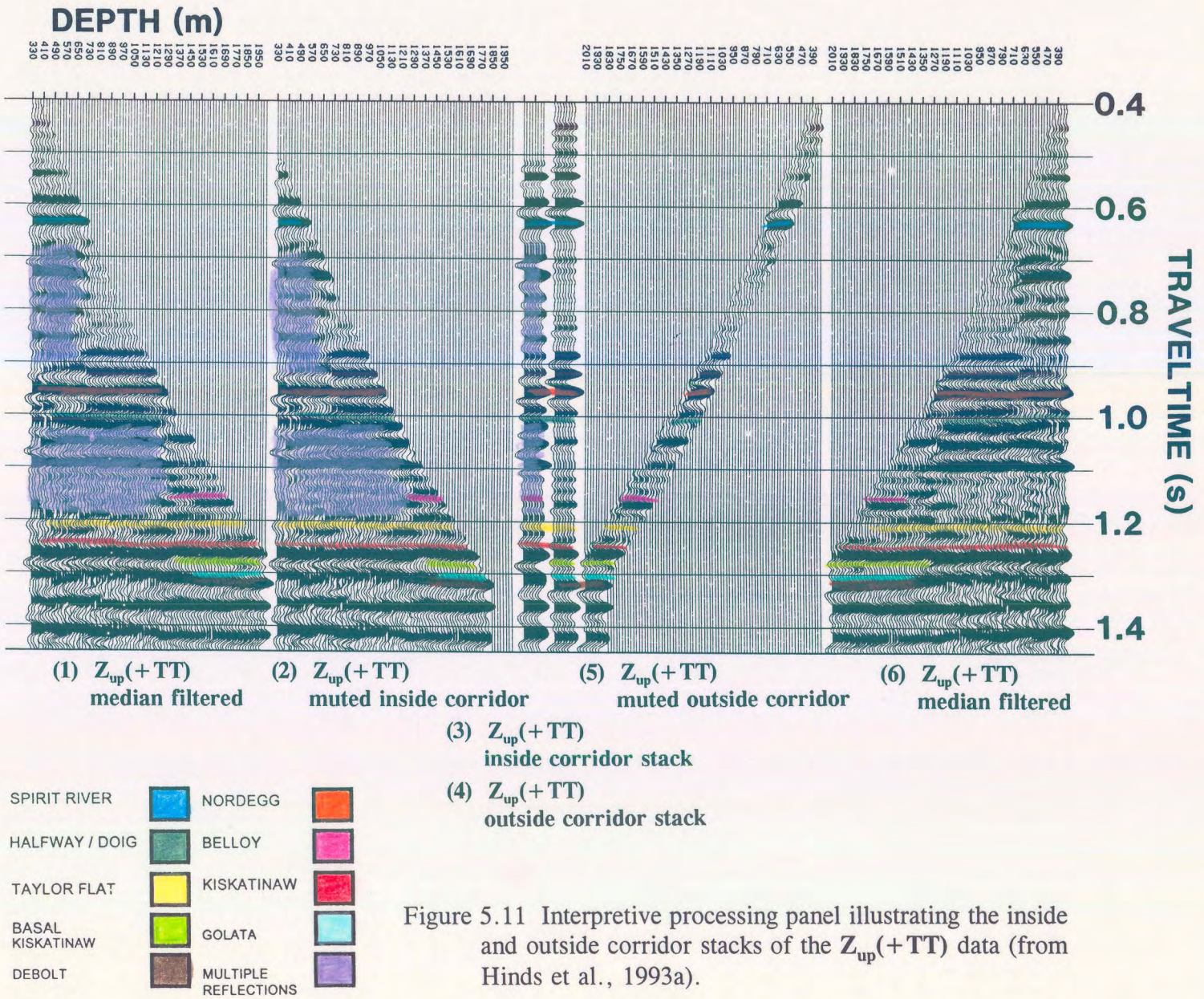

Figure 5.11 Interpretive processing panel illustrating the inside and outside corridor stacks of the $Z_{up}(+TT)$ data (from Hinds et al., 1993a).

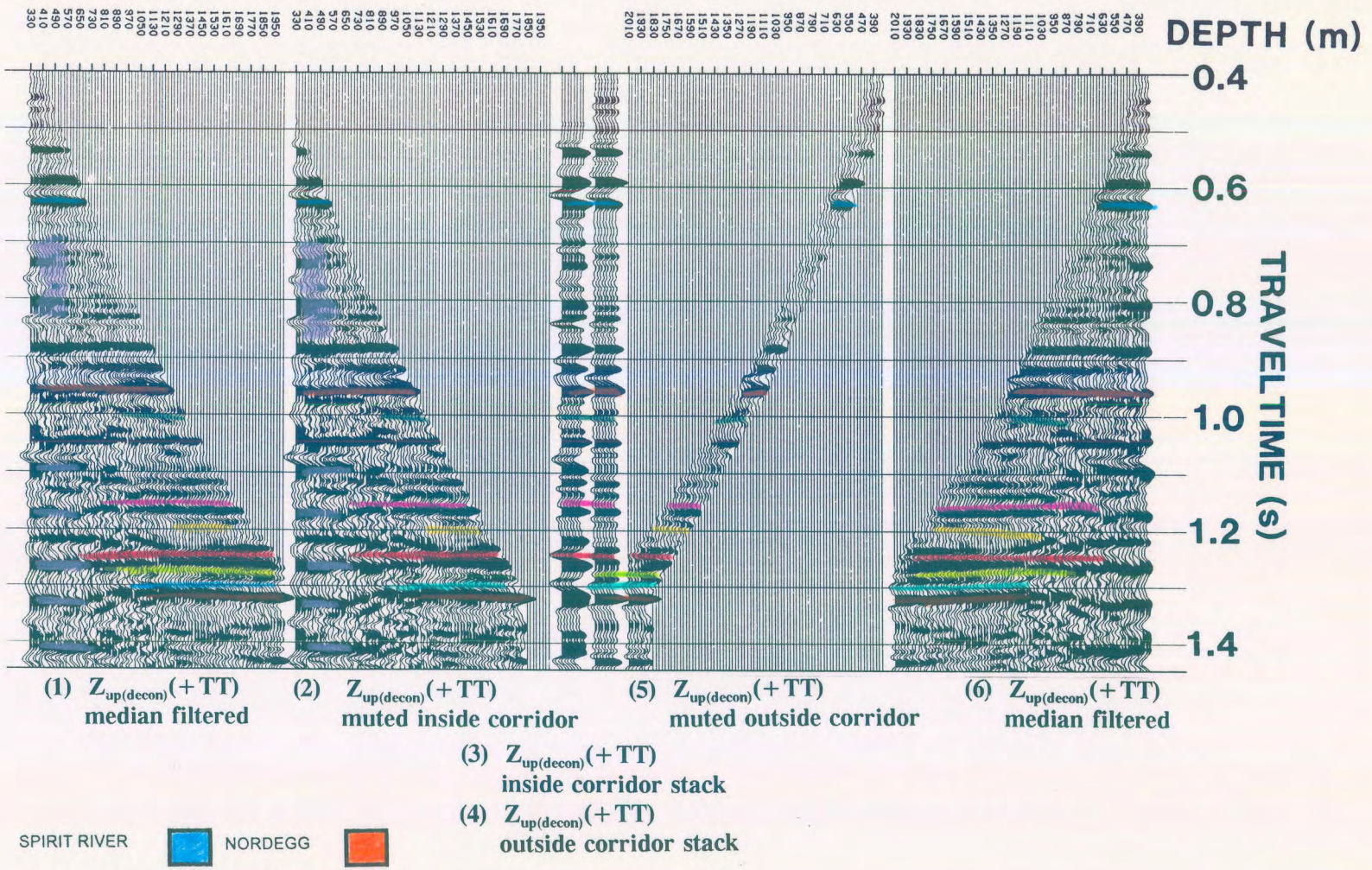

Figure 5.12 Interpretive processing panel illustrating the inside and outside corridor stacks of the $Z_{up(decon)}(+TT)$ data (from Hinds et al., 1993a).

contamination has not been completely eliminated on the shallow traces (from 1290 m to the surface). This results in a broad peak for the zone immediately above the basal Kiskatinaw (on panel 3 at 1.26 s) but the high frequency basal Kiskatinaw trough has been overpowered by residual multiple contamination. Note that the Spirit River multiple which is highlighted in purple between 0.65 and 1.0 s has been significantly attenuated on all of the traces except for the traces recorded at 490 m to the surface. The deconvolution process has given limited success; however the data can be correlated to the geology and later to the surface seismic.

5.6 Far offset VSP interpretive processing

5.6.1 Far offset data from offset FSJG1

On the far offset FSJG1 VSP data, the vertical (**Z**) and both horizontal (**X** and **Y**) axis data contain nonpartitioned elements of the upgoing and downgoing P- and SV-wavefields. Examination of the IPPs (Figs. 5.13-5.15) reveals that the partitioning of the wavefields has significant implications with respect to interpretation (Hinds et al., 1989a). The far offset IPPs for the FSJG1 data (Hinds et al., 1993a; Hinds et al., 1994c) were designed with the aim of displaying the following major processing steps:

1) hodogram-based rotation of the **X(FRT)**, **Y(FRT)**, and **Z(FRT)** data (based on windowed data enveloping the P-wave first arrival; DiSiena et al., 1984);

2) time-variant model-based rotations applied to the $\mathbf{HMAX_{up(derot)}(FRT)}$ and $\mathbf{Z_{up(derot)}(FRT)}$

data; and

3) VSP-CDP mapping (Dillon and Thomson, 1984) and Kirchhoff migration processing (Dillon, 1990; Wiggins and Levander, 1984; Wiggins et al., 1986; Wiggins, 1984) of the $\mathbf{Z''_{up}(+TT)}$ data.

5.6.2 Hodogram-based rotation; offset FSJG1

The **X(FRT)**, **Y(FRT)**, and **Z(FRT)** data for the FSJG1 far offset VSP are displayed in Figure 5.13 on panels 1, 2, and 3, respectively. The horizontal axis data (**X** and **Y**) are extremely noisy and contain only minor amounts of P-wave events. The **Z(FRT)** data contain strong downgoing P-wave events plus lower amplitude upgoing P-wave events. The hodogram-based rotation technique is designed to polarize these data so that the downgoing P-waves are presented on a single channel, **HMAX'(FRT)**.

The first step illustrated in Figure 5.13, is the hodogram-based rotation of the **X(FRT)** and **Y(FRT)** data (correcting for phase changes due to tool rotation during the movement of the sonde up the borehole). The output **HMIN(FRT)** and **HMAX(FRT)** data are displayed as panels 4 and 5, respectively. **HMIN(FRT)** and **HMAX(FRT)** data are assumed to be aligned perpendicular and tangent to the plane formed by the well and the source, respectively. Note that the **HMIN(FRT)** data (comprised of horizontally polarized shear (SH) wave events and out of the plane reflections) contains the dominant portion of the diffraction that appears at 1.0s on the 650 to 800 m traces, suggesting that the diffraction is side-swipe energy originating from a feature such as a fault out of the plane of the well and source.

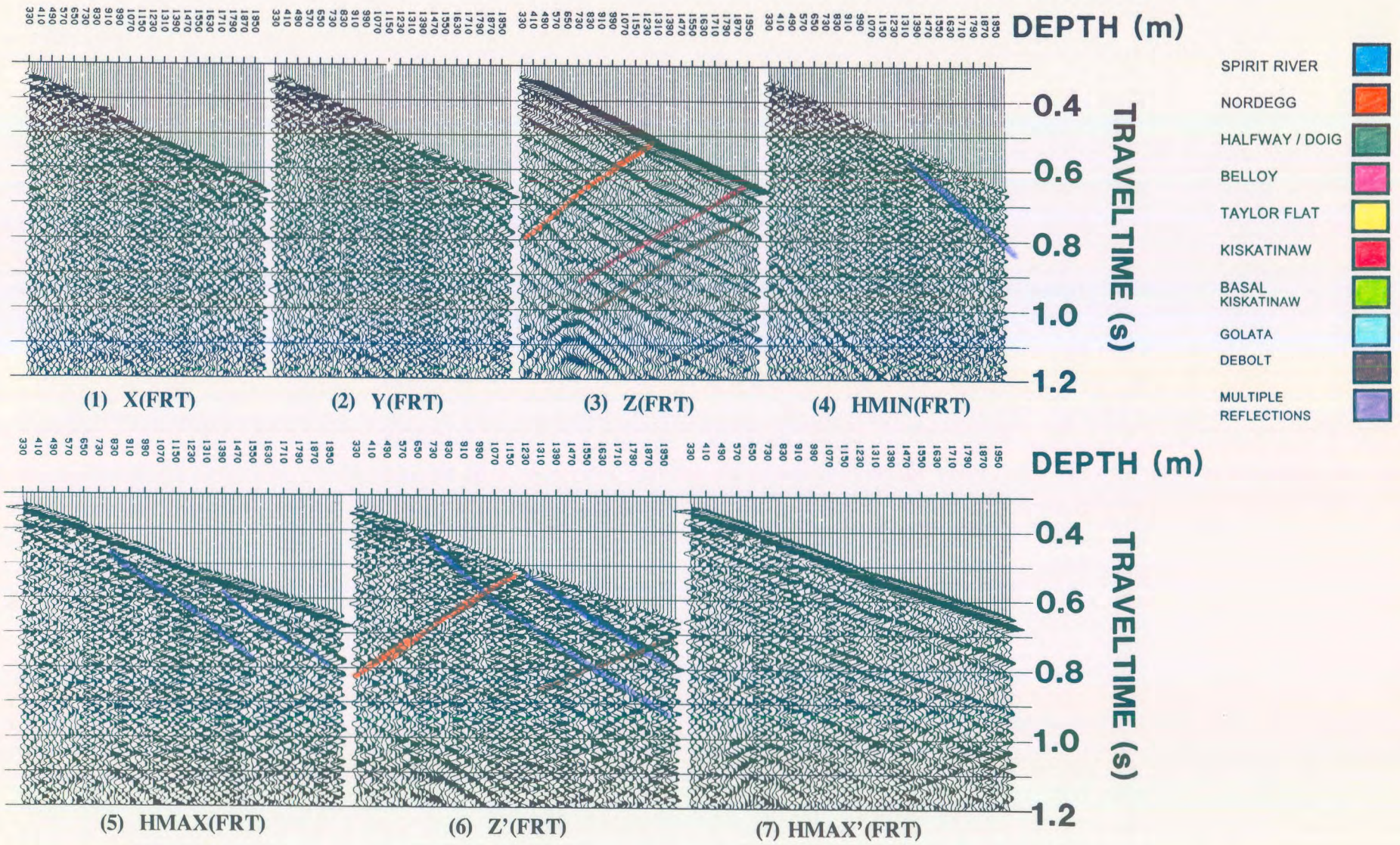

Figure 5.13 Interpretive processing panel depicting the hodogram-based rotation of the Fort St. John Graben FSJG1 far offset VSP data (from Hinds et al., 1993a).

The **Z'(FRT)** and **HMAX'(FRT)** (panels 6 and 7) data were obtained by rotating the **Z(FRT)** and **HMAX(FRT)** data using polarization angles estimated from a hodogram analysis of a window of data centred around the P-wave first arrivals of the **Z(FRT)** and **HMAX(FRT)** data (DiSiena et al., 1984). Downgoing mode-converted SV-events can be interpreted on all three axis data, **X(FRT)**, **Y(FRT)** and **Z(FRT)**. The SV-events were described for these data in chapter 2. The SV data can be used for the quality control of the second polarization; namely, **HMAX(FRT)** and **Z(FRT)** data rotating into **HMAX'(FRT)** and **Z'(FRT)** data.

The evaluation of the second polarization is based on the detection or not of SV-events (mode-converted or from any other origin) on the **HMAX'(FRT)** data. In panel 6 and 7 of Figure 5.13, the mode-converted SV events have been completely polarized onto the **Z'(FRT)** data and, at first inspection, do not appear on the HMAX'(FRT) data.

The upgoing events on VSP data can be up to 100 times weaker than the downgoing events (Hardage, 1985). The time-variant polarization IPP (Fig. 5.14) that have been designed and presented in the next section contains the wavefield separated **Z'$_{up}$(FRT)** and **HMAX'$_{up}$(FRT)** data in panels 1 and 2, respectively. It is only after the wavefield separation processing on the **Z'(FRT)** and **HMAX'(FRT)** data that the underlying upgoing event components of the **Z'(FRT)** and **HMAX'(FRT)** data can be truly evaluated.

The two sets of rotations have polarized the **X(FRT)**, **Y(FRT)** and **Z(FRT)** data so that the downgoing P-waves are effectively isolated on a single channel, **HMAX'(FRT)**, shown in panel 7 of Figure 5.13.

5.6.3 Time-variant model-based rotation: offset FSJG1

The IPP for the time-variant model-based polarization analysis for the FSJG1 offset data is shown in Figure 5.14. The **Z'$_{up}$(FRT)** and **HMAX'$_{up}$(FRT)** are shown in panels 1 and 2 (Fig. 5.14), respectively. On both panels, upgoing P-waves from the Debolt, Golata and Kiskatinaw can be clearly interpreted, indicating that the hodogram-based rotations were unsuccessful in isolating the upgoing P-wave events onto the **Z'(FRT)** panel.

In order to remove the effects of the **Z(FRT)** to **Z'(FRT)**, and **HMAX(FRT)** to **HMAX'(FRT)** transformations (which were necessary to isolate the downgoing P-waves), the **Z'$_{up}$(FRT)** and **HMAX'$_{up}$(FRT)** were derotated (using the inverse operation of the second polarization rotation). The **Z$_{up(derot)}$(FRT)** and **HMAX$_{up(derot)}$(FRT)** data, are shown as panels 3 and 4 of Figure 5.14, respectively. By inspection, the upgoing P-wave events have been effectively distributed back onto a Z-type axis data, **Z$_{up(derot)}$(FRT)**. Unlike the upgoing wave events in the **Z(FRT)** data (panel 3 in Fig. 5.13), where the downgoing P-waves were predominant, the separated upgoing P-wave events in the **Z$_{up(derot)}$(FRT)** data are dominant and interpretable.

On the **Z$_{up(derot)}$(FRT)** data (panel 3), upgoing P-waves generated by the shallow reflectors are improperly aligned (due to the choice of a single rotation angle per trace) such as the upgoing event resulting from the reflection from the Spirit River interface. These data have been derotated but the upgoing P-wave events are still partitioned on both output data (**Z$_{up(derot)}$(FRT)** and **HMAX$_{up(derot)}$(FRT)**) due to the non-zero offset of the source. The deeper events do not suffer much misalignment because the deep event raypath geometries

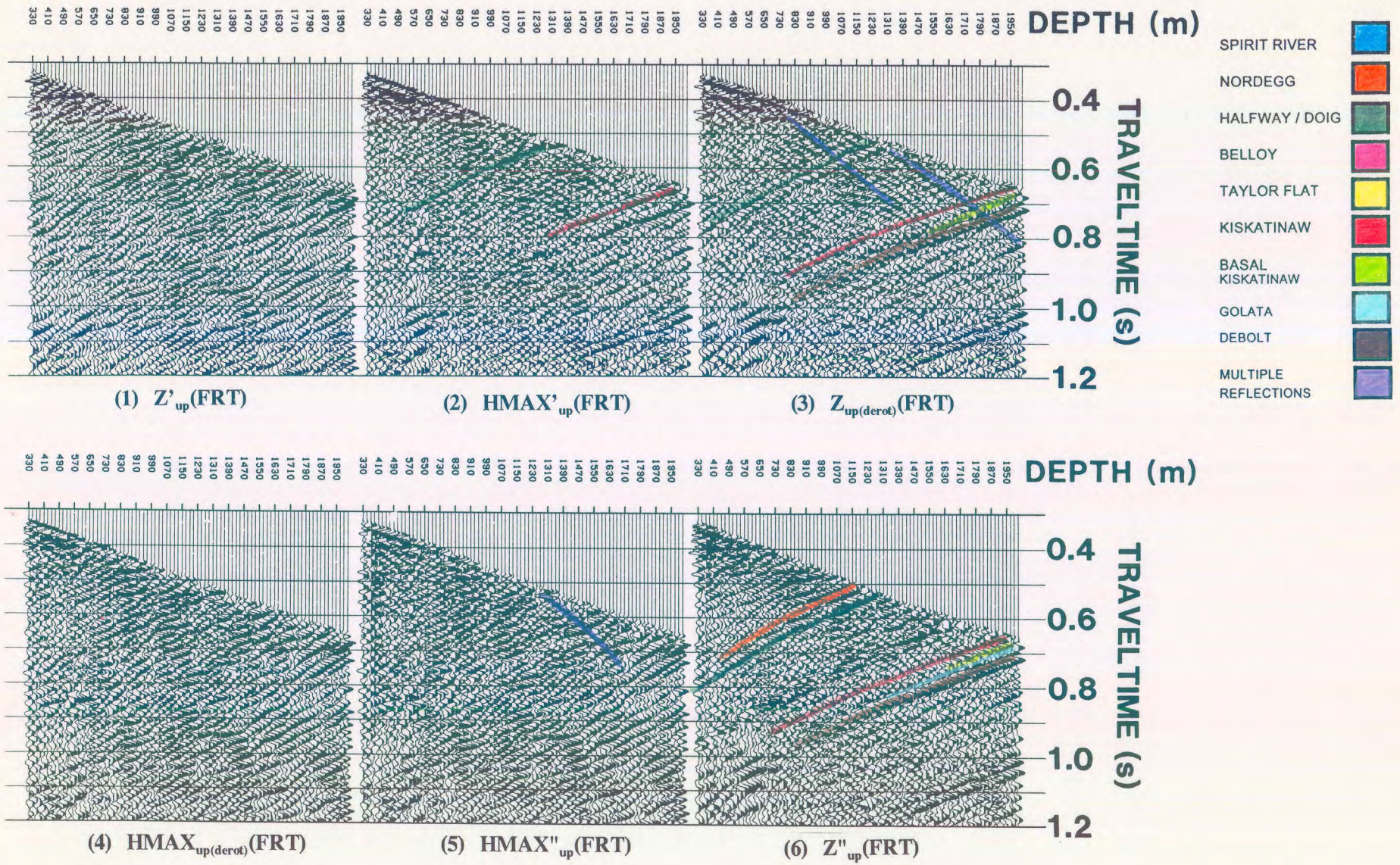

Figure 5.14 Interpretive processing panel depicting the time-variant model-based rotation of the Fort St. John Graben FSJG1 far offset VSP data (from Hinds et al., 1993a).

satisfy the near-vertical incidence angle assumption better than the raypaths of shallower events. The time-variant model-based rotation corrects for this misalignment. The output of the time-variant polarization, the **HMAX"$_{up}$(FRT)** and **Z"$_{up}$(FRT)** data, are shown in panels 5 and 6, respectively. Note that the shallow events display more alignment than on the **Z$_{up(derot)}$(FRT)** (panel 3). The rotation angle required for the Spirit River and Nordegg events on a particular trace are different to the rotation angle needed for a deeper event (such as the Debolt) on the same trace. The time-variant rotation technique (Hinds et al., 1989a) generated these different rotation angles.

The Spirit River event is barely discernable on the **Z"$_{up}$(FRT)** data because the reflected raypaths from this shallow event are at or near the critical angle. The surface-generated multiple from the Spirit River interface (observed on the nondeconvolved near offset data of panel 7 in Fig. 5.9) are significantly lower amplitude on these far offset data (panel 6; Fig. 5.13).

5.6.4 VSP-CDP mapping: offset FSJG1

Nonfiltered and median-filtered **Z"$_{up}$(FRT)** data are displayed (pseudo-two-way traveltime versus depth) in figure 5.15 as panels 1 and 2, respectively. The VSP-CDP mapped (pseudo-two-way traveltime versus offset) and Kirchhoff migrated **Z"$_{up}$(+TT)** data are shown as panels 3 and 4, respectively.

The FSJG1 offset source was located 700 m and in the direction of well 2-25. The interpretation of the surface seismic data (Fig. 5.8) suggests that a major Debolt fault

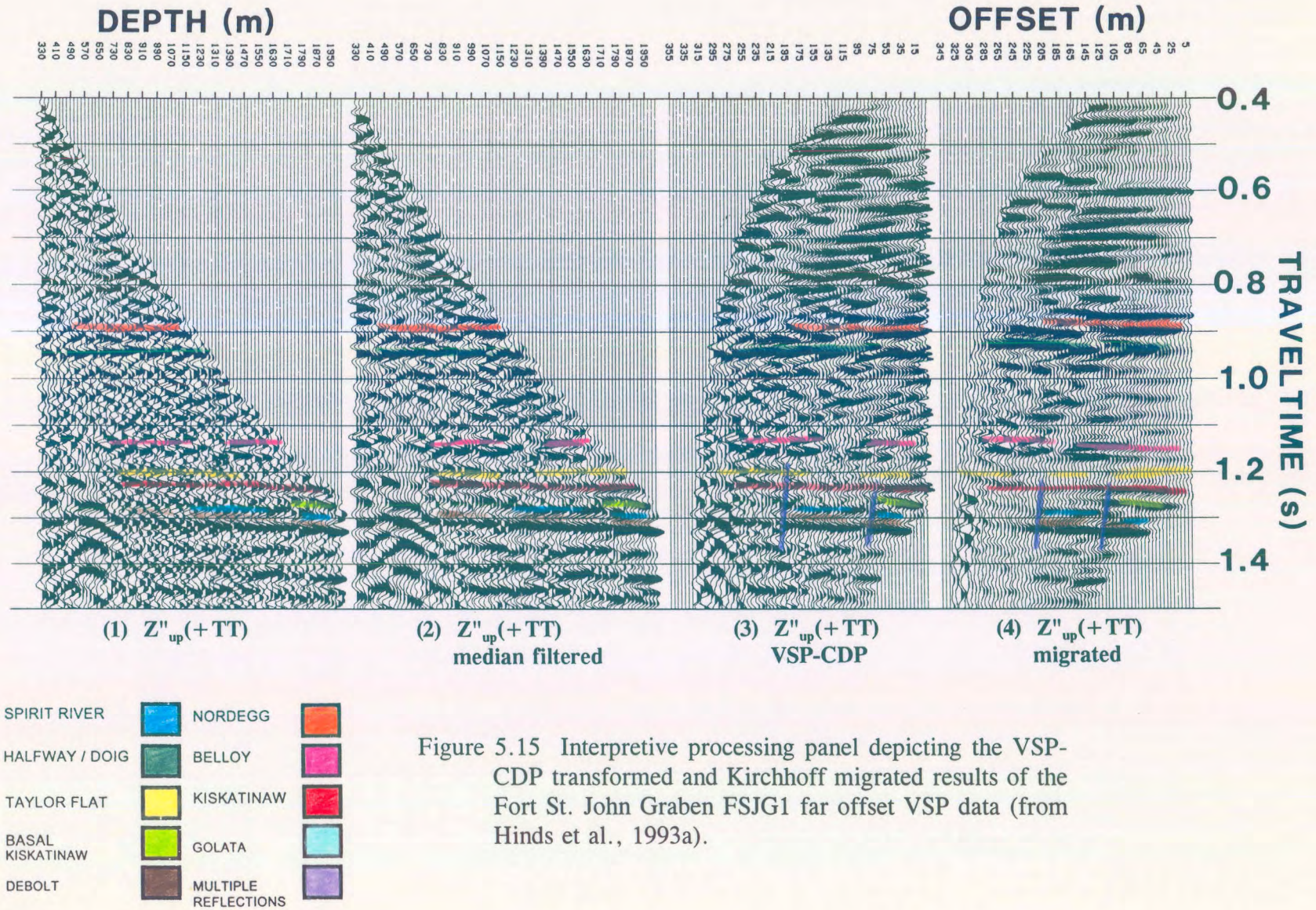

Figure 5.15 Interpretive processing panel depicting the VSP-CDP transformed and Kirchhoff migrated results of the Fort St. John Graben FSJG1 far offset VSP data (from Hinds et al., 1993a).

(displacing Debolt to the Belloy Fm material) was located between well 9-24 and well 2-25. On panels 3 and 4 (Fig. 5.15), the Debolt event on the VSP data is interpreted to be faulted in two places in between these wells; however, it is shown in section 5.7 that these VSP data image two faults not shown on the interpretation on Figure 5.8 (Hinds et al., 1994b).

A second interesting feature on panel 3 is that the signature of the basal Kiskatinaw event changes abruptly in proximity to the fault nearest well 9-24. The migrated version has smeared the event. The basal Kiskatinaw event, as interpreted, is continuous at greater offsets, but is substantially decreased in amplitude. This character change could indicate a change in lithology (increase in shale content) or porosity (increase in water content as in well 2-25).

The upper Kiskatinaw event which represents the location of the hydrocarbon reservoir within well 9-24 is interpreted on panels 3 and 4 to be laterally continuous but faulted. Vertical displacement is interpreted across two faults. This thesis is supported by geological information (Richards, pers. comm.); the upper Kiskatinaw is present in both wells 9-24 and 2-25. At well 9-24 the upper Kiskatinaw forms a gas reservoir; in the structurally higher 2-25 well this unit is nonproductive.

5.6.5 Far offset data from offset FSJG2

The FSJG2 far offset source was 741 m east of well 9-24. These data were acquired in order to map the lateral extent of the upper Kiskatinaw reservoir to the east of well 9-24, and to provide a higher resolution seismic image of faults that displace Debolt strata. The offset

survey was designed in an effort to explore a new area in which future exploration could be realized. This is a case where the VSP data capture is done before a possible seismic survey can be performed in the area. The recording and processing of these data was similar to that described for the FSJG1 survey.

In the first stage of interpretive processing, a hodogram-based rotation technique polarized the **X(FRT)**, **Y(FRT)**, and **Z(FRT)** data, so that the downgoing P-waves were presented on a single channel, **HMAX'(FRT)** as shown in Figure 5.16. The filtered output data, **Z'$_{up}$(FRT)** and **HMAX'$_{up}$(FRT)**, were derotated and time-variant model-based rotations were applied to the output data as shown in Figure 5.17. In the final stage, the **Z"$_{up}$(FRT)** data were displayed in pseudo-two-way traveltime versus depth, and in pseudo-two-way traveltime versus offset.

The **Z"$_{up}$(+TT)** data after the application of the VSP-CDP mapping are displayed in Figure 5.18. Nonmedian and median-filtered versions of the **Z"$_{up}$(+TT)** data are displayed (pseudo-two-way traveltime versus depth) as panels 1 and 2, respectively. The VSP-CDP mapped (pseudo-two-way traveltime versus offset) and Kirchhoff migrated **Z"$_{up}$(+TT)** data are shown in panels 3 and 4, respectively.

The data in panels 3 and 4 image 2 faults, both of which are of the same magnitude as those on the FSJG1 data (Fig. 5.15). The basal Kiskatinaw event is interpreted to exhibit a laterally continuous seismic signature. This is unlike the character of the basal Kiskatinaw

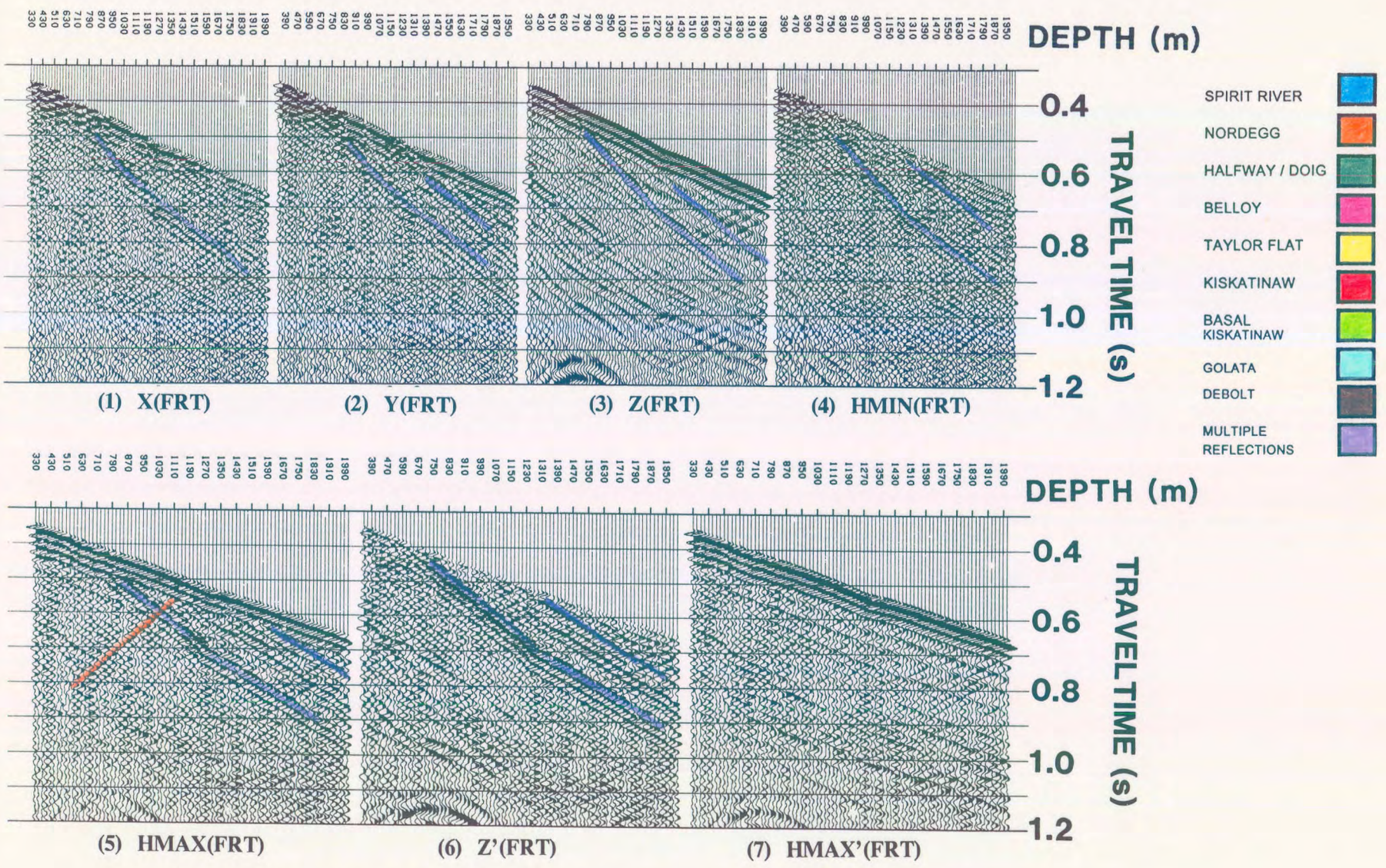

Figure 5.16 Interpretive processing panel depicting the hodogram-based rotation of the Fort St. John Graben FSJG2 far offset VSP data (from Hinds et al., 1993a).

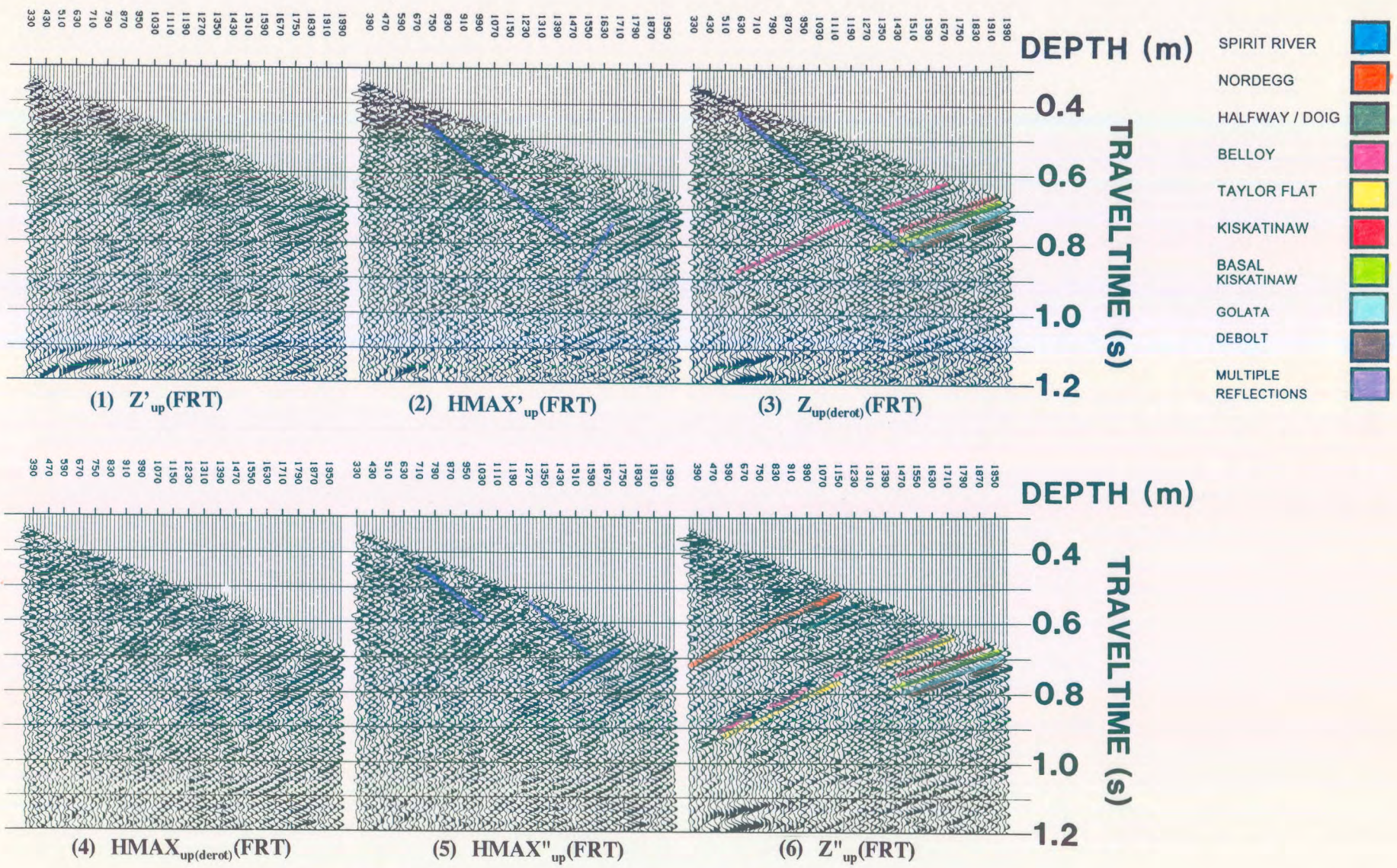

Figure 5.17 Interpretive processing panel depicting the time-variant model-based rotation of the Fort St. John Graben FSJG2 far offset VSP data (from Hinds et al., 1993a).

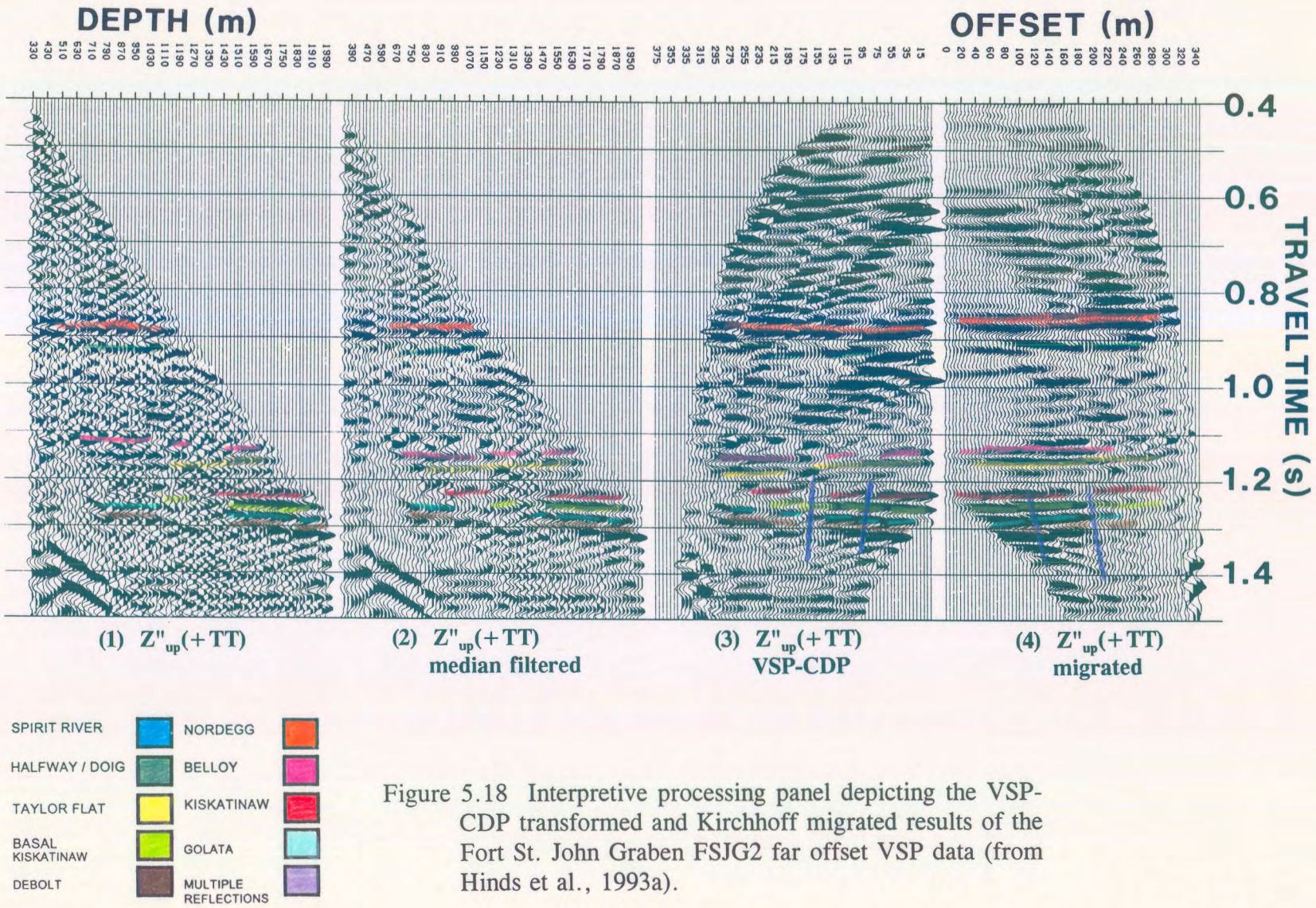

Figure 5.18 Interpretive processing panel depicting the VSP-CDP transformed and Kirchhoff migrated results of the Fort St. John Graben FSJG2 far offset VSP data (from Hinds et al., 1993a).

away from the well towards the FSJG1 offset source which decreases in amplitude beyond the first imaged fault. The upper Kiskatinaw (hydrocarbon reservoir at well 9-24), as interpreted on panel 3, is laterally continuous but faulted.

5.7 Integrated interpretation

The integrated interpretive display (IID) is shown in Figure 5.19. On the left-hand side of the IID (from Hinds et al., 1993a; Hinds et al., 1994c) in Figure 5.19, gamma ray logs for the well 9-24, well 2-25, and well 7-36 are time-tied to the current interpretation of the surface seismic data. On the right-hand side, near offset VSP data are time-tied to the gamma ray and sonic logs acquired in well 9-24. These correlated data allow for the confident interpretation of the surface seismic line and the identification of the Spirit River, Nordegg, Halfway/Doig, Belloy, Taylor Flat, upper Kiskatinaw, basal Kiskatinaw, Golata, and Debolt events. The nondeconvolved version of the VSP data is presented, in order to facilitate an analysis of multiple contamination. As evidenced by a comparison of the surface seismic line and the corridor stacks, the multiple-contaminated inside corridor stacks provide a poor tie to the data at the zone of interest (Kiskatinaw). This suggests that multiples on the surface seismic data have been effectively attenuated.

The interpretation of the surface seismic section that incorporates the VSP information (normal polarity display; Fig. 5.20) differs slightly from the pre-well interpretation (Fig. 5.8). Of particular significance is that on the updated version, the Taylor Flat and Kiskatinaw events are confidently correlated. Note that in the post-VSP interpretation, the Taylor Flat event is absent at well 7-36. This interpretation is supported by the well log

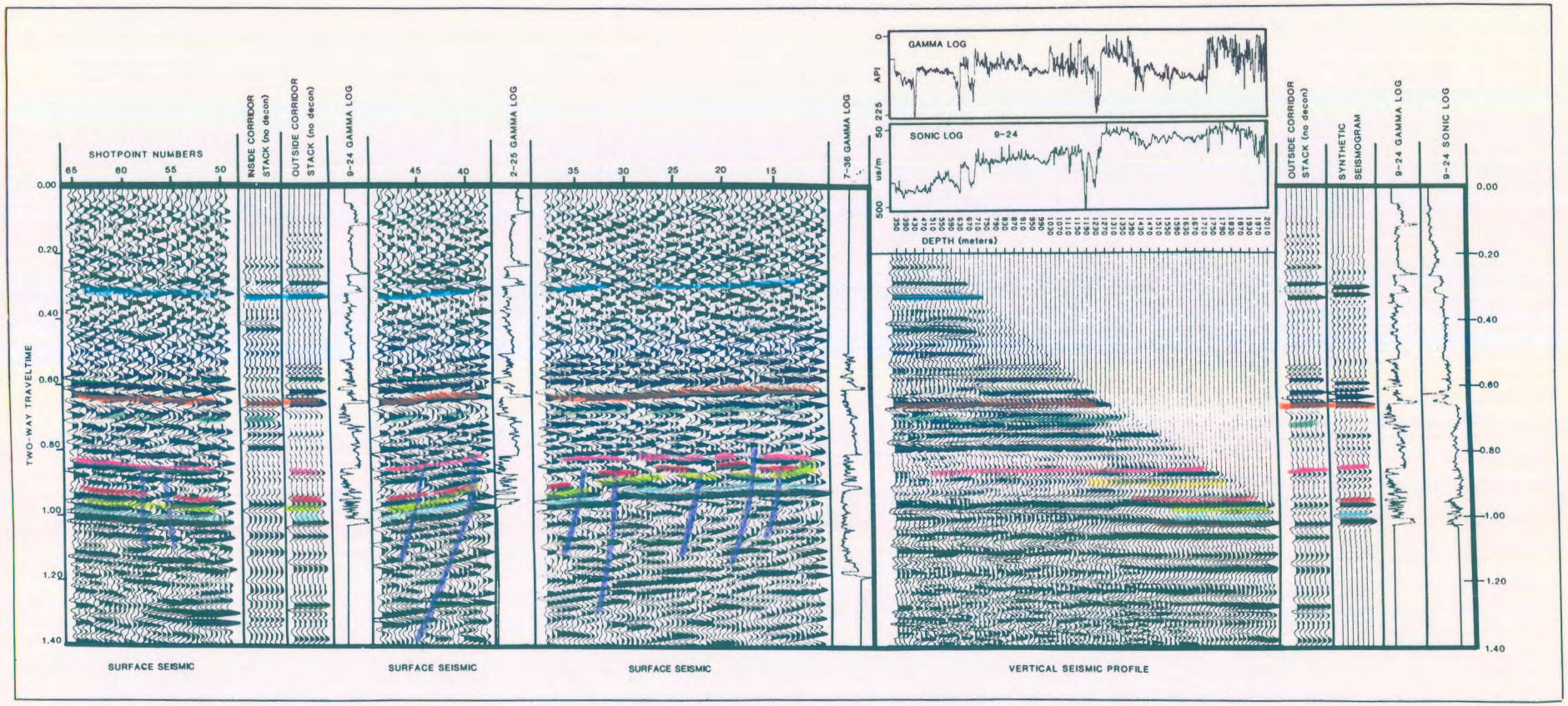

Figure 5.19 Integrated interpretive display of the Fort St. John Graben exploration data (from Hinds et al., 1993a).

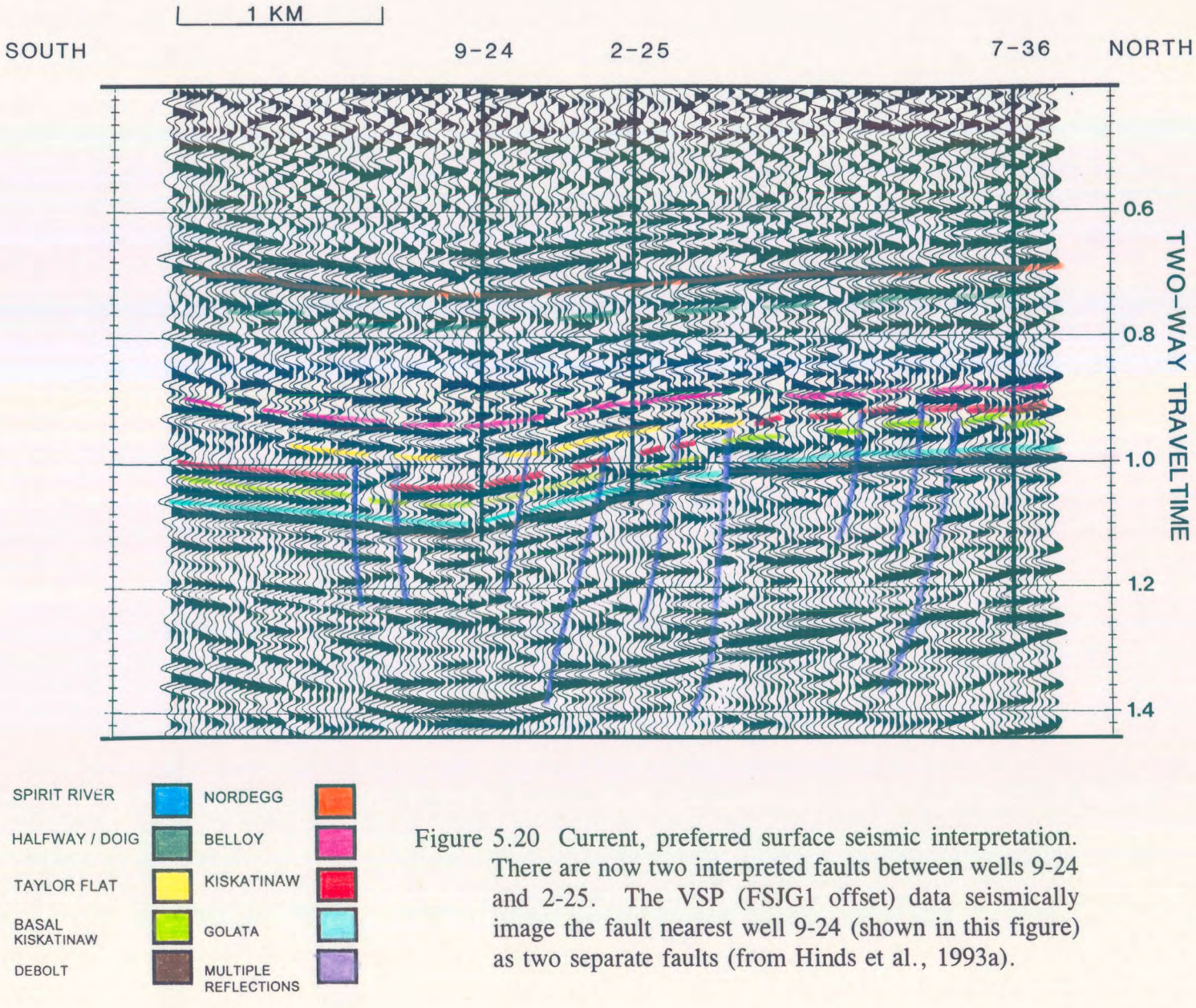

Figure 5.20 Current, preferred surface seismic interpretation. There are now two interpreted faults between wells 9-24 and 2-25. The VSP (FSJG1 offset) data seismically image the fault nearest well 9-24 (shown in this figure) as two separate faults (from Hinds et al., 1993a).

control.

The geologic cross-section of Figure 5.21 was constructed on the basis of the post-VSP interpretation of the surface seismic line and the analysis of the far offset VSP data. It is consistent with the well log, surface seismic and seismic profile control. Up-to-date information using conodont research and lithostratigraphic data (Richards, pers. comm.) is shown in Figure 5.21 as Upper Carboniferous strata informally known as the Ksituan Member of the Taylor Flat Formation (Hinds et al., 1994b and Hinds et al., 1994c). This geologic cross-section is an update to the one presented in Hinds et al. (1993a) and is discussed in Hinds et al. (1994b) and Hinds et al. (1994c).

A discrepancy that arose and was resolved in Hinds et al. (1994b) came about from the observation that there are two faults interpreted on the VSP-CDP data shown in Figure 5.15 and three faults between well 9-24 and well 2-25 on the geologic cross-section shown in Figure 5.21. In addition, on the reinterpreted seismic data, shown in Figure 5.20, there are two faults interpreted between wells 9-24 and 2-25. The two faults interpreted on the VSP-CDP data do not correlate with the interpreted fault shown on Figure 5.8 (between wells 9-24 and 2-25); these interpreted faults (Fig. 5.15) are represented on the reinterpreted seismic data (Fig. 5.20) as a single fault near to well 9-24. The surface seismic data could not resolve the seismic expression of the fault into two separate images as seen on the VSP-CDP data (Fig. 5.15).

In Hinds et al. (1994b), a plan view of the FSJG1 source offset position along with the location of the two VSP interpreted faults and surface seismic located fault (near well 2-25)

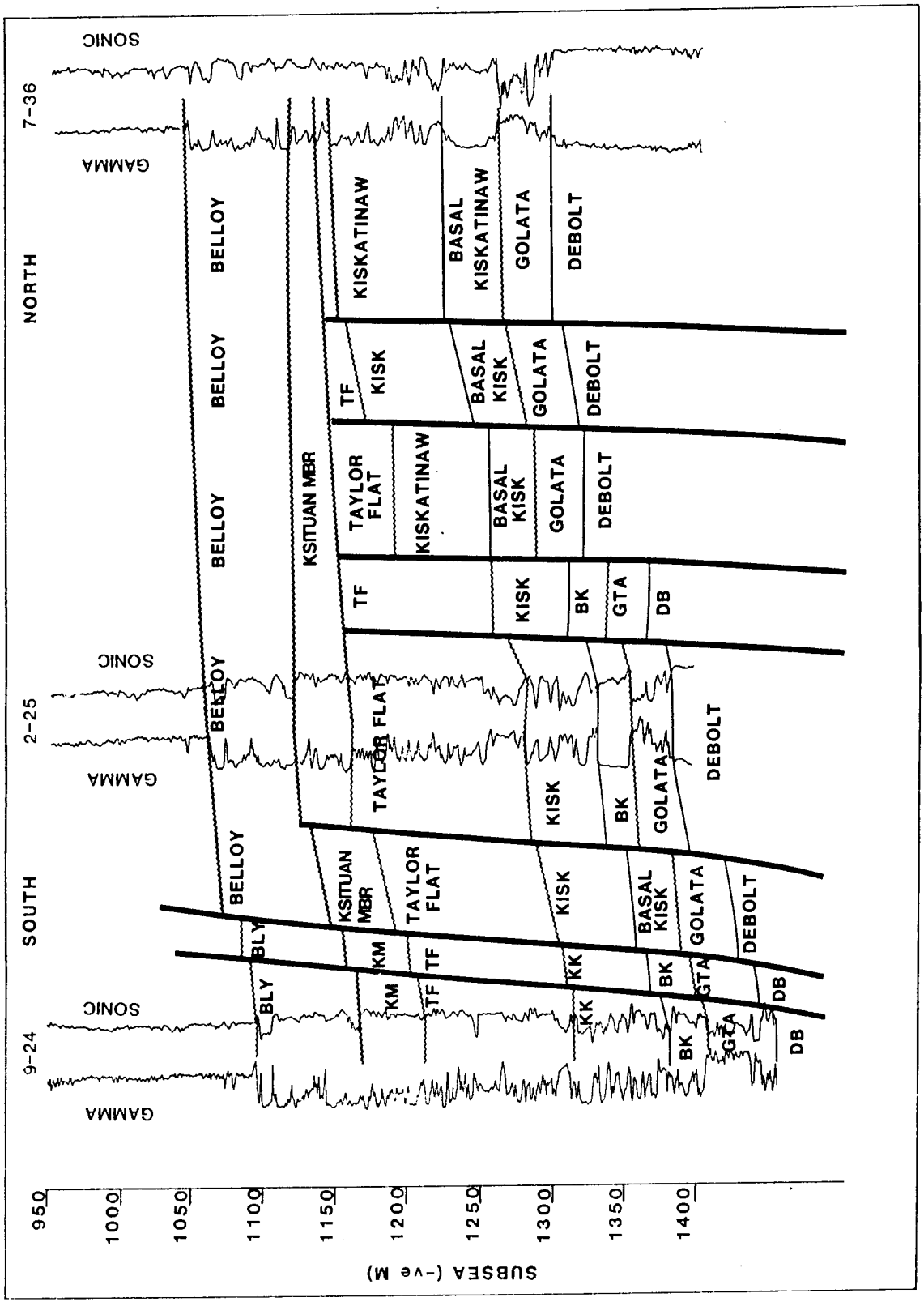

Figure 5.21 Geologic cross-section incorporating information from the surface seismic, VSP and geologic well log results (from Hinds et al., 1994c). Note that three faults have been postulated to be between wells 9-24 and 2-25.

was discussed and is shown in Figure 5.22 (Hinds et al., 1994c). This presentation of the VSP and surface seismic line geometry aids in the resolution of the discrepancy discussed in Hinds et al. (1994b). In Figure 5.22, well 9-24 is located due East of CDP number 49 of the seismic line shown in Figures 5.8 and 5.20. The far offset source location is marked by a circle to the northwest of the well 9-24 location. The subsurface coverage of the VSP-CDP data extends along a direction towards the offset source location starting at well 9-24 out to half the distance from well 9-24 to the source. The two VSP illustrated faults on the seismic line nearest well 9-24 project onto the seismic line at CDP numbers 47 and 48. These faults are shown as a single fault on the reinterpreted seismic line in Figure 5.22. The layout in Figure 5.21 clearly shows that the fault displayed on the seismic line immediately South of well 2-25 is not imaged on the VSP-CDP data; only on the seismic data. In this case, the VSP-CDP interpretation has brought new information into the integrated interpretation.

5.8 Conclusion

The exploratory well 9-24 was drilled on the downthrown side of a fault block on the basis of conventional surface seismic data. The expectation was that the gas-prone sandstones of the basal Kiskatinaw Fm would be truncated laterally and sealed against the upthrown fault-block. Contrary to expectations, the basal Kiskatinaw was unproductive; however, well 9-24 did encounter commercial gas within the upper Kiskatinaw which was now shut-in.

Figure 5.22 Plan map of the FSJG1 offset source area showing the fault locations as interpreted from the VSP and surface seismic data (from Hinds et al. 1994c). The VSP data (FSJG1 far offset) imaged the two faults along the seismic line nearest to well 9-24 and the seismic imaged the fault nearest to well 2-25. These two datasets complement each other in the construction of the geological interpretation shown in Figure 5.21.

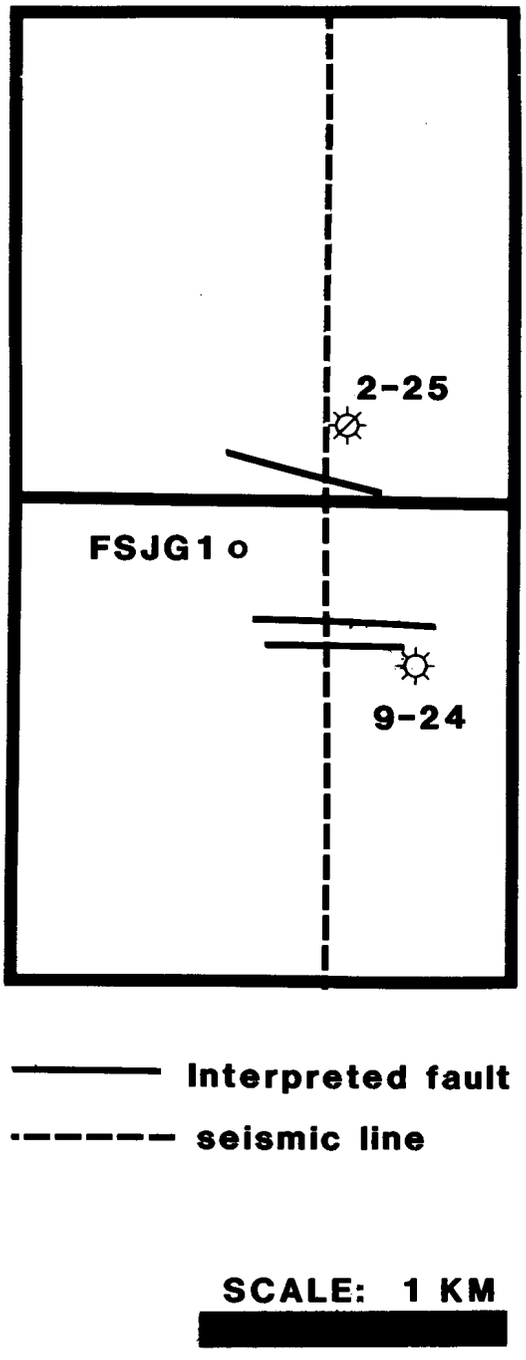

To obtain a high resolution seismic image of the subsurface in the vicinity of well 9-24, and to evaluate the proximity of any displacements features such as faults which might not have been resolved on the surface seismic data, three VSP surveys were designed and run on the 9-24 well-site. This seismic profiling information, in conjunction with surface seismic coverage, was used to image the subsurface fault pattern, and elucidate the seismic signature and lateral continuity of the upper Kiskatinaw Fm strata. The profile data supplemented the surface seismic and well log control in that VSP data could be directly correlated to the surface seismic data. As a result, the surface seismic control could be accurately tied to the subsurface geology; multiples could be identified on the VSP data and evaluated on the surface seismic data; and the subsurface, in the vicinity of the borehole, was better resolved on the VSP data than on the surface seismic control.

The information provided by the VSP surveys allowed this work to provide a refinement of the interpretation of the surface seismic data, and enabled the construction of a detailed geologic cross-section (Fig. 5.21). These interpretations provide information with respect to the subsurface in proximity to well 9-24, and perhaps more importantly, further elucidate the geologic history of the structurally complex Fort St. John Graben area (Richards et al., 1994).

CHAPTER 6

SIMONETTE REEF CASE STUDY

On the basis of conventional surface seismic data, the 13-15-63-25 W5M exploratory well was drilled into a low relief Leduc Formation reef (Devonian Woodbend Group) in the Simonette area, west-central Alberta, Canada. The well was prognosed to intersect the crest of the reef and to encounter about 50-60 m of pay; unfortunately, it was interpreted later to have intersected a flank position of the reef and was abandoned. The decision to abandon the well, as opposed to whipstocking in the direction of the reef crest, was made after the acquisition and interpretive processing of both near and far offset (252 and 524 m, respectively) vertical seismic profile (VSP) data, and after the reanalysis of existing surface seismic data.

The VSP survey was designed, performed and the results of a near and far offset VSP survey interpreted while the drilling rig remained on-site, with the immediate objectives of: (1) determining an accurate tie between the surface seismic data and the subsurface geology; and (2) mapping relief along the top of the reef over a distance of 150 m from the 13-15 well location in the direction of the adjacent productive 16-16 well with a view to whipstocking. These surveys proved to be cost effective in that the operator of the well was able to determine that the crest of the reef was out of the target area, and consequently that whipstocking was not a viable alternative. The use of VSP surveys in this situation allowed the owners of the well to avoid the costs associated with whipstocking, and to have

confidence about their decision to abandon the well.

In this chapter, the 2-D surface seismic and VSP signatures of the low-relief reef in the Simonette study area (Hinds at al., 1993b and 1994c) are discussed with a view to obtaining a refined seismic image at the VSP-well and in the surrounding area . The 2-D data were acquired prior to drilling the 13-15 exploratory well which ultimately ended up intersecting the reef in a flank position below the oil/water contact as interpreted in this chapter. The initial processing of the raw VSP data was done by Vector Technology in 1987. The interpretive processing results presented in this chapter represent a more extensive treatment of all of the exploration data including the VSP data (taken from raw input data) and shown in Hinds et al (1993b).

6.1 Simonette Field

The Simonette Reef lies within the western Woodbend depositional realm (Stoakes and Wendte, 1987) where the reef environment is slightly different to that of the southeastern realm (Moore, 1989a). The southeastern realm included the geology for the case studies described in chapters 3 (Lanaway/Garrington field) and 4 (Ricinus field). A short review is presented below.

The Woodbend Group in central Alberta (Figs. 3.1A, B, and C) is subdivided into four formations: Cooking Lake, Duvernay, Leduc, and Ireton. In the Simonette study area of the western Woodbend depositional realm, the Cooking Lake Formation is depositionally absent and the Leduc Formation conformably overlies the Beaverhill Lake Group (Moore, 1989a).

The Leduc reef in the Simonette study area (Hinds et al., 1993b and 1994c) developed as both full and low-relief reef. The areal extent of the full reef which towers up to 230 m above the Beaverhill Lake platform, is defined roughly by the 70 m Ireton isopach contour interval in Figure 6.1. In Figure 6.1, the position of a geologic profile is shown defined by 8 wells with the corresponding geologic cross-section defined by the geophysical logs being shown in Figure 6.2.

Within the cross-section, well 10-34 penetrated the calcareous muds of the interior lagoon facies of the Leduc reef and was abandoned. Well 04-06 was drilled as a development well and is currently classified as an oil well although operations of producing from the well have been suspended. Well 10-06 was drilled into the northeastern portion of the Simonette atoll reef and is a flowing oil well. Well 04-16 was drilled into the raised peripheral rim (Anderson, 1986) and is a flowing oil well. The inter-reef well 10-16 was drilled off the rim of the main Simonette reef and penetrated only Ireton and Duvernay shales. Well 10-16 was abandoned. The five wells mentioned above were all drilled in the period 1960-62 when the Simonette Field was being developed in Alberta. Through numerous wells, the field was delineated and an Ireton isopach contour map (Hinds et al., 1993b) is shown in Figure 6.1 where the reef is interpreted to exist where the carbonates displace the encasing shales resulting in low shale isopach values.

Wells 16-16 and 04-22 were drilled in the period 1986-89 and are described in the next section. The final well shown in the geologic cross-section is the well 08-34 (a well in the shale basin) which did not encounter carbonate rocks of the Leduc Formation but was drilled through Ireton and Duvernay shales and Beaverhill Lake reef platform facies down to the Elk

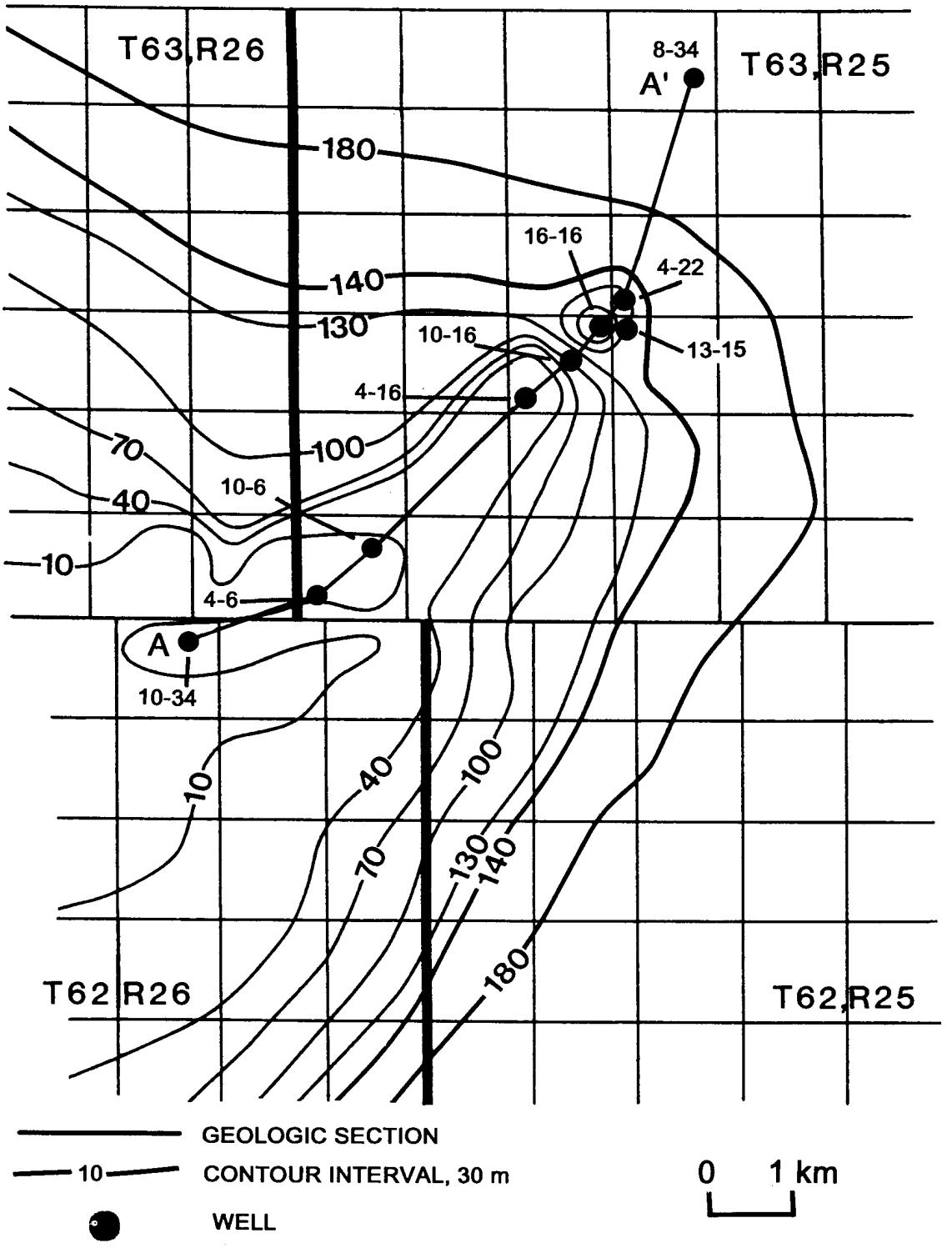

Figure 6.1 Ireton isopach map of the main and low-relief Simonette reef within the eastern Woodbend depositional realm. The locations of the wells used in the construction of the geologic cross-section shown in Figure 6.2 are shown in this figure. The exploratory well 13-15 is also posted (from Hinds et al., 1993b and 1994c).

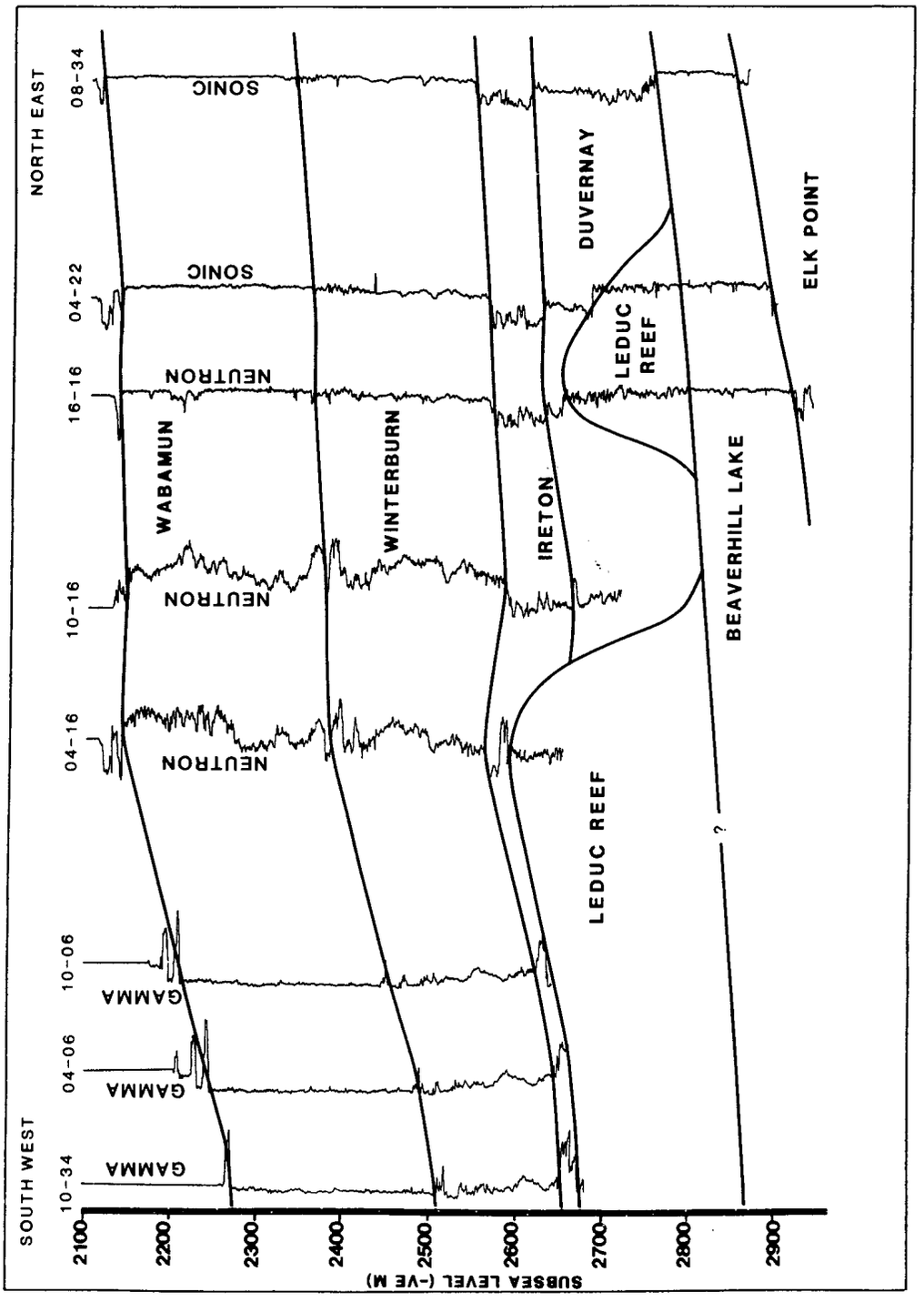

Figure 6.2 Geologic cross-section A-A' traversing the wells shown in Figure 6.1. The traverse starts in the southwest on the main Simonette reef at the back-reef lagoonal facies well, 10-34; continues to the northeast on the main reef for wells 4-6, 10-6, 4-16; into inter-reef shales for well 10-16; onto the low-relief reef with wells 16-16 and 4-22; and into the shale basin in well 8-34 (from Hinds et al., 1993b and 1994c).

Point Formation. The borehole logs within Figure 6.2 consist of neutron, gamma and sonic logs. The cross-section (Hinds et al., 1993b) shows the morphology of the Wabamun, Winterburn, Ireton, Leduc, Beaverhill Lake and Elk Point Formations and displays the placement of the study area reef (comprising of wells 16-16, 04-22 and the VSP-well, 13-15) with respect to the main Simonette atoll reef.

The low-relief reef of the study area, in contrast to the development of full reef buildup, attains a maximum thickness on the order of 120 m; its approximate areal extent is defined by the 130 m contour interval (Sections 15, 16, 21 and 22 of Township 63, Range 25 W5M; Fig. 6.1). The study area reef examined in this chapter is an isolated carbonate buildup that is basinward of the main Simonette atoll. The up-dip edges of both types of carbonate buildups can be productive where they are structurally closed and effectively sealed by the inter-reef shales of the Duvernay and Ireton Formations.

The term full reef was used in Anderson et al., (1989) to describe atolls and adjacent pinnacles which attain a height of over 200 m (Figs. 6.1 and 6.2) and is readily mapped on good quality 2-D seismic data; it is characterized by appreciable velocity pullup in the order of 30 ms, time structural drape of about 30 ms at the top of the Devonian (Wabamun Formation), and character variations within the Woodbend interval (the Leduc, Ireton and Duvernay Formation seismic events). The seismic signature of the low-relief reef which was the target of the VSP-well, as evidenced by the example seismic data (Fig. 6.3), is more subtle, being manifested by less than 15 ms of pullup and less than 15 ms drape of the Wabamun event from reef to off-reef. In addition, the reflection from the top of the low-relief reef can be difficult to distinguish from the Z-marker (an inter-reef shale event used

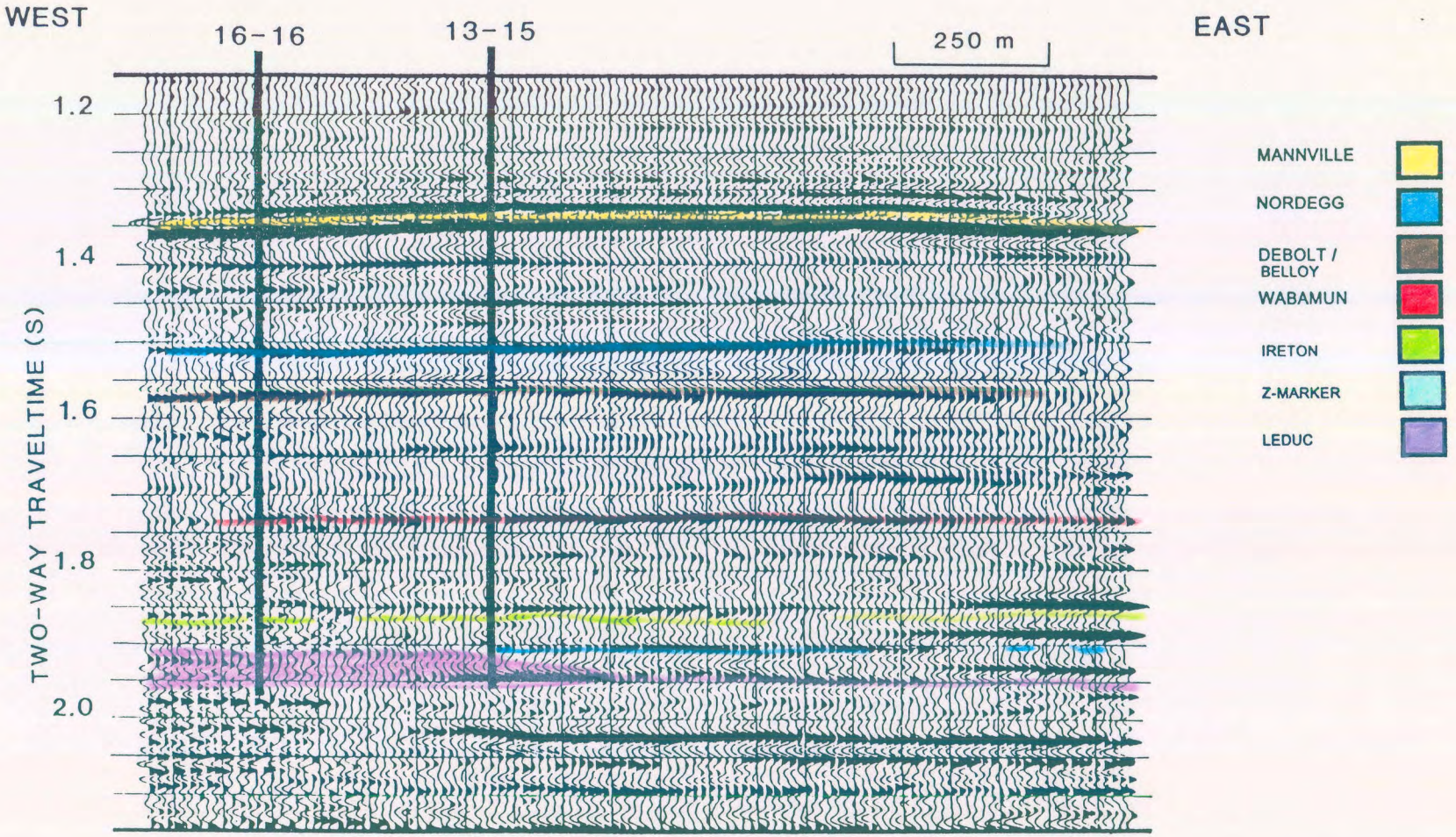

Figure 6.3 Example surface seismic data over the low-relief reef displaying the original interpretation of the owner of the data. The interpretation was done prior to the drilling of the well (from Hinds et al., 1993b and 1994c).

in the interpretation of seismic data in the Simonette atoll area; Hinds et al., 1993b). On Figure 6.3, an event beneath the reef at 2.2 s "pulls up" starting 8 traces East of the 13-15 well location (as shown on Fig. 6.3). This pullup suggested that the edge the low-relief reef could be located as indicated in Figure 6.3.

6.2 Simonette low-relief reef

Three wells penetrate the low-relief carbonate buildup seen as a northeast extension of the main Simonette reef in Figure 6.1; namely, 16-16-63-25 W5M, 4-22-63-25 W5M, and 13-15-63-25 W5M. Well 16-16 encountered 72 m of net pay; well 4-22 encountered 24 m of net pay but watered out after 12 months of production; well 13-15 is the abandoned exploratory well for which the two VSPs were acquired (see Fig. 6.4 for the three well locations).

The contour map of the Ireton to Leduc isochrons which was derived from the originally interpreted seismic data (interpreted by the owners of the seismic data) is shown in Figure 6.4. The prognosis was that well 13-15 would encounter 50-60 m of net pay. The contour map of Figure 6.5 summarizes the final preferred evaluation derived from the thesis work for the 13-15 location using the drilling results, the interpretation of the near and far offset nondeconvolved and deconvolved VSP data, and the reinterpretation of the suite of existing surface seismic lines within the area.

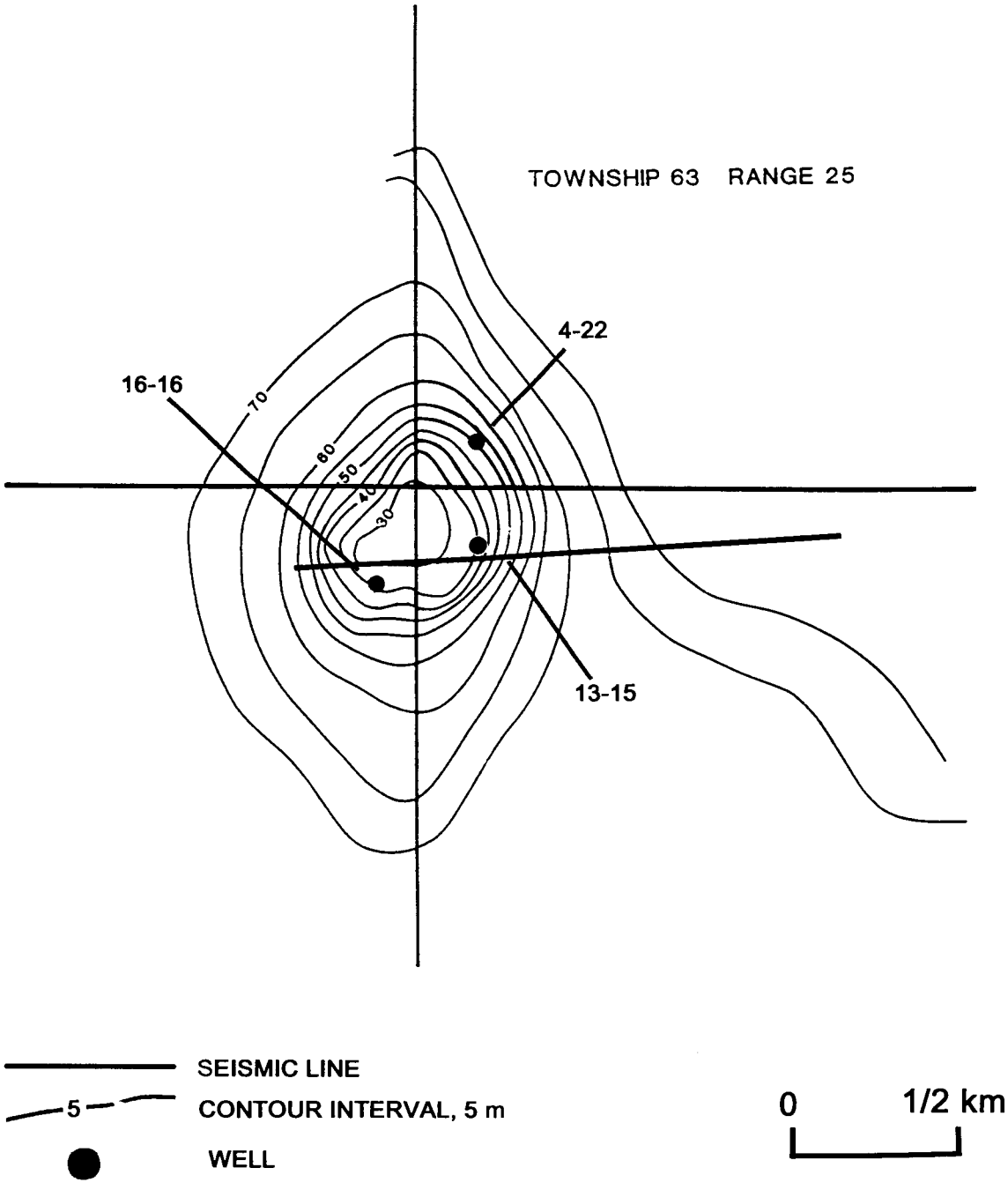

Figure 6.4 Ireton to Leduc isochron map resulting from the original interpretation of the seismic lines within the area of the low-relief reef. The oil pay-zone of the low-relief reef is interpreted to be as productive at the proposed well 13-15 as at the existing well 16-16 (from Hinds et al., 1993b, 1994c).

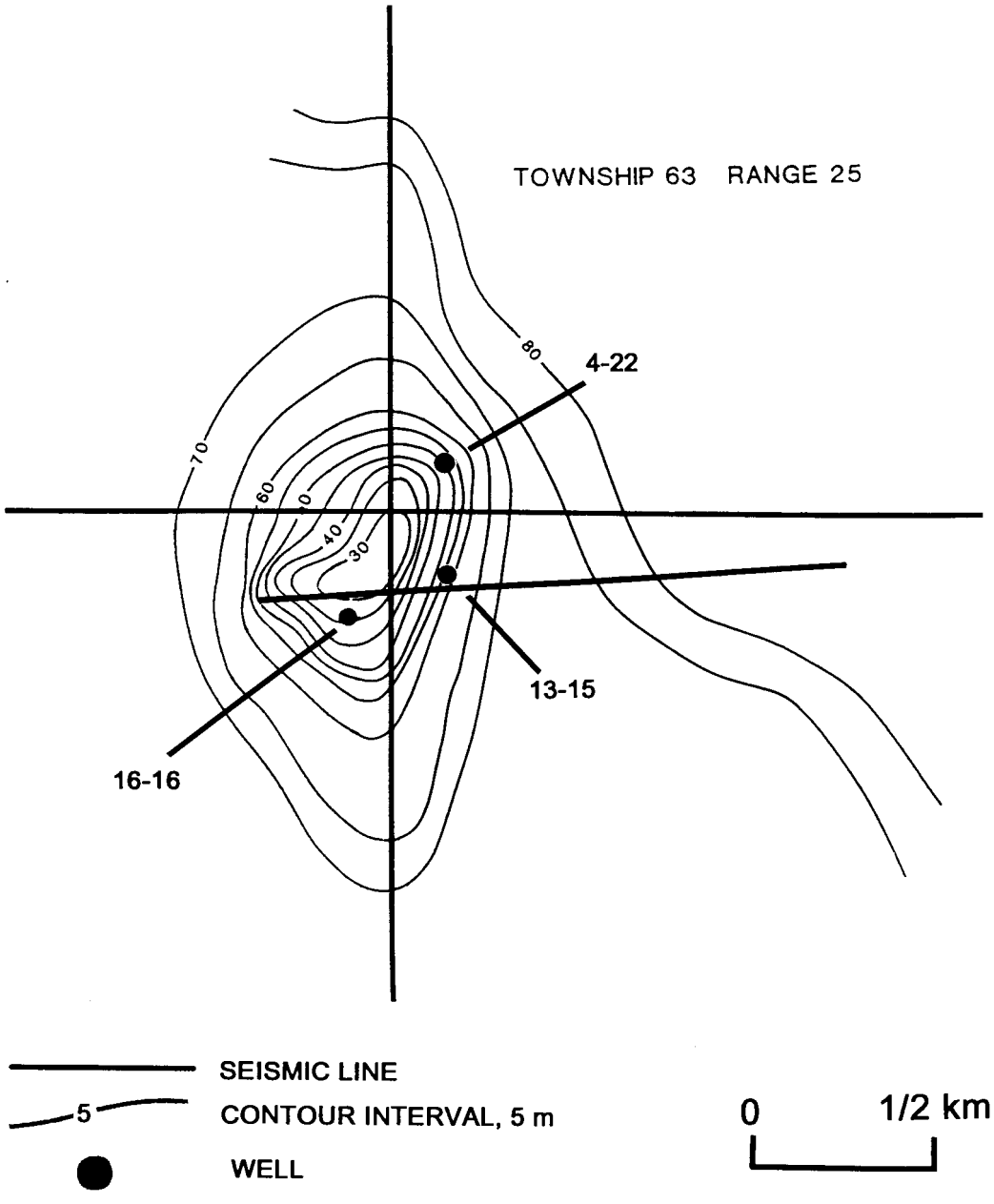

Figure 6.5 The preferred Ireton to Leduc isochron resulting from the updated interpretation (using the VSP results) of the seismic lines in the area of the low-relief reef, the VSP results and geologic borehole data. This interpretation shows the reef gradually rising out to 120 m from well 13-15 and then steeply rising towards well 16-16 (from Hinds et al., 1993b and 1994c).

The surface seismic line (normal polarity display; Fig. 6.3) is a stack of nominally 20-fold, split-spread, 120 prestack trace data, acquired using a patterned dynamite source (2 X 0.5 kg at 9 m depth; shotholes spaced 25 m apart) and DFS-5 recording equipment (8-128 hz filter). The seismometer groups consisted of nine, inline, 14 hz geophones spaced at 3.75 m. The geophone group and shot intervals were 25 and 75 m, respectively.

The seismic markers of principal interest correspond to the Mannville, Nordegg, Debolt/Belloy, Wabamun, Ireton, Z-marker (a regional marker within the inter-reef shales), and Leduc (Figs. 6.2 and 6.3). The Z-marker corresponds to the top of the Duvernay shales listed in the stratigraphic chart in Figure 6.2 and is caused by a change in the carbonate content within the Duvernay shale versus the overlying Ireton shale. The seismic image of the subsurface at well 13-15 (Fig. 6.3), was initially interpreted as comparable to that at the productive well 16-16 location; hence it was drilled. The high-amplitude event at about 1.9 s, at the 13-15 location, was mistakenly interpreted as the top of the reef. In retrospect, it is believed to be the off-reef Z-marker. Well 13-15 intersected the low-relief reef in a flank position below the oil/water contact (P. Pelletier, pers. comm.) and encountered 134 m of inter-reef shale (in comparison with 75 m of shale encountered in well 16-16). On the basis of the well results, it was suggested that the low-relief reef could rise abruptly to the west and that whipstocking in the direction of the productive 16-16 well should be considered.

The operators of well 16-16 were left with two alternatives: abandon the well or whipstock in the direction of well 16-16, bearing in mind that the further well 13-15 deviated from the original bottomhole location, the greater the Alberta Government imposed production penalty. In order to ascertain the cost-effectiveness of whipstocking the operators ran two VSP

surveys: a near offset (252 m) and a far offset (524 m) VSP survey. It was on the basis of these data and the reinterpretation of the existing surface seismic, that the decision was made to abandon well 13-15 without any whipstock.

6.3 VSP acquisition

After an analysis of the 13-15 well geophysical logs and prior to abandonment, two VSP surveys were run at this well site in order to:

1) more accurately tie the surface seismic data and an interpretation thereof to the subsurface geology (in particular the top of the low-relief Leduc reef);

2) map the top of the reef over a distance of 150 m in the direction of the 16-16 well (with a view to whipstocking); and

3) differentiate primary reflections from both surface-generated and interbed multiples.

The near offset was chosen to be 252 m from well 13-15, the far offset to be 524 m; both are online with respect to the surface seismic line (Fig. 6.4). Two Vibroseis units were operated in series at each offset. The 12 s sweep ranged from 10 to 70 hz, the recording length was 15 s, and the cross-correlated output was 3 s. On average, six sweeps were summed for each geophone sonde location. MDS-10 recording instruments and a sampling interval of 1 ms were used. The recording filter was OUT/250; the instrument filter served

as an anti-aliasing, lowpass filter with a ramp rolloff starting at 250 hz.

Well 13-15 extends 3620 m below the Kelly Bushing (at 878 m asl). Both source locations were at 868 m asl. The geophone sonde was lowered to the bottom of the well and raised at 20-30 m intervals. At each sonde location, the three component geophone tool was locked in place.

The two offsets were designed to be within the direction of the producing 16-16 well with the following interpretation considerations in mind:

1) if the slope of the reef was steep, a diagnostic seismic signature would be seen of the 252 m offset data; however a diagnostic shadow zone (null data) would be seen on the 524 m data;

2) if the crest was not steep but gradual, then both offset data would reflect the seismic image of the slope (the 252 m offset data would be a subset of the 524 m offset VSP data); and

3) if the slope was gradual but became steeper beyond the range of the near offset (252 m) VSP, then the 252 and 524 m offset data would both image the gradual slope but only the longer offset data would image the steeply sloped part of the reef.

6.4 Near offset (252 m) VSP interpretive processing

During the processing of the near offset VSP, a series of interpretive processing panels (IPPs) were designed (Hinds et al., 1993b and 1994c) to display the following :

1) separation of $\mathbf{Z_{up}(FRT)}$ and $\mathbf{Z_{down}(FRT)}$ data from the **Z(FRT)** data;

2) deconvolution of the $\mathbf{Z_{up}(FRT)}$ data to output the $\mathbf{Z_{up(decon)}(FRT)}$ using an inverse filter calculated from the $\mathbf{Z_{down}(FRT)}$ data; and

3) inside and outside corridor stacks (Hinds et al., 1989a) of both the $\mathbf{Z_{up}(+TT)}$ and $\mathbf{Z_{up(decon)}(+TT)}$ data.

6.4.1 P-wave separation

The separation of the upgoing and downgoing P-waves on the vertical (**Z**) geophone data is illustrated in the wavefield separation IPP (Hinds et al., 1989a) in Figure 6.6.

Panel 1 (Fig. 6.6) displays the normalized **Z(FRT)** data. In panel 2, high-amplitude surface-generated multiples, and less prominent interbed multiples can be seen in the **Z(-TT)** data. The surface-generated downgoing multiples can be recognized as continuous events arriving after the first break primary downgoing wavetrain on all of the traces, from the deepest to the shallowest receiver location (Hinds et al., 1989a). A downgoing multiple associated with

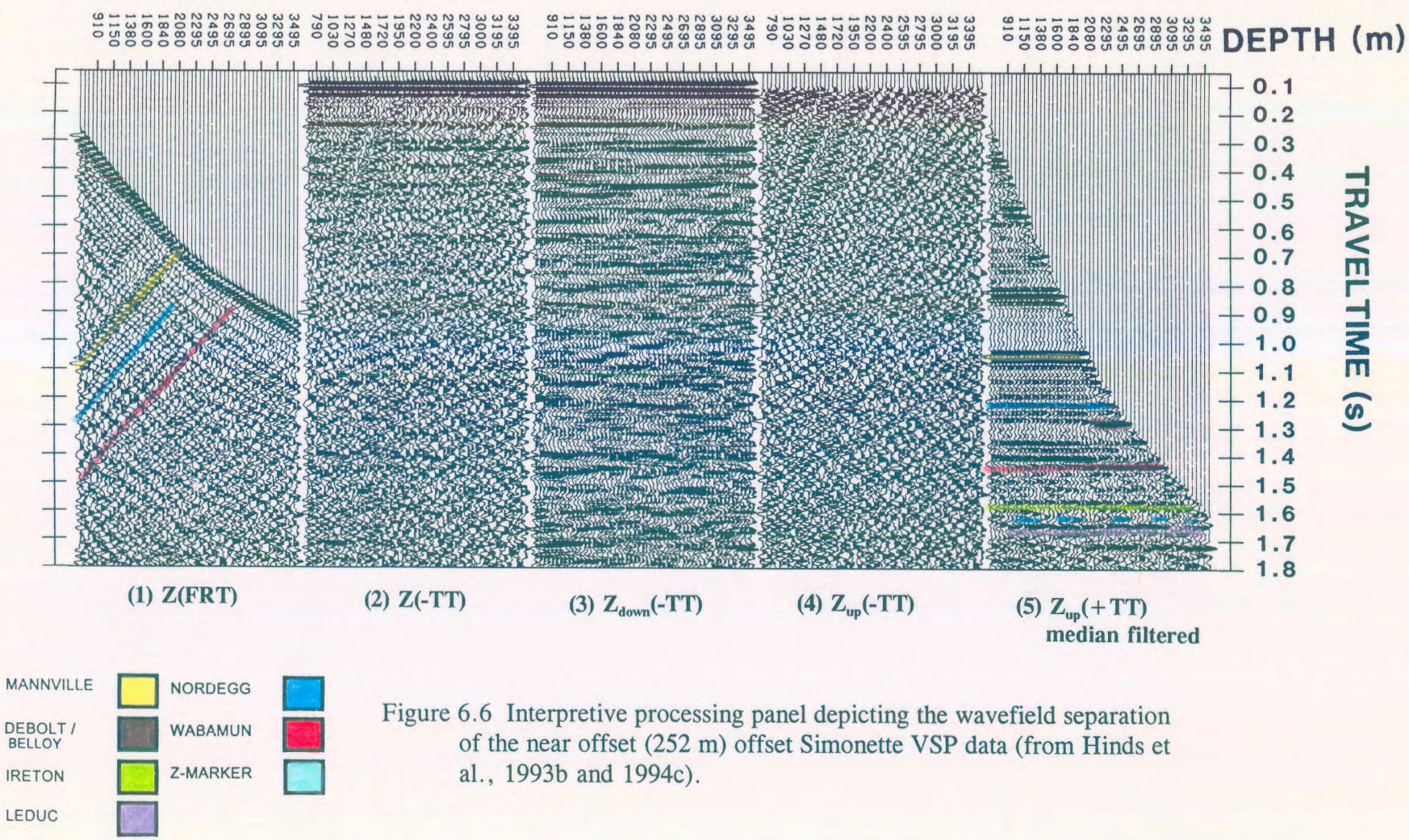

Figure 6.6 Interpretive processing panel depicting the wavefield separation of the near offset (252 m) offset Simonette VSP data (from Hinds et al., 1993b and 1994c).

the Mannville Formation interface is interpreted to start at the 2080 m trace (between 0.3 and 0.32 s; panel 2) and continue onto the deeper traces. The event may be an interbed multiple, since on panel 2, it does not appear to continue onto the shallower depth traces. The $\mathbf{Z_{down}(-TT)}$ data in panel 3 do not assist in the interpretation since the median filter has smeared the event onto the shallower traces. An inspection of the $\mathbf{Z_{up}(+TT)}$ data in panel 5 confirms that multiple interference is definitely originating from the Mannville Formation top interface.

The $\mathbf{Z_{down}(-TT)}$ data were obtained from the **Z(-TT)** data using an eleven-point median filter and are displayed in panel 3. The residual $\mathbf{Z_{up}(+TT)}$ data content in panel 3 are interpreted to be minimal since the data consist predominately of horizontally aligned downgoing events. The $\mathbf{Z_{up}(-TT)}$ shown in panel 4 were separated from the **Z(-TT)** data by subtracting the $\mathbf{Z_{down}(-TT)}$ as reviewed in chapter 2. The Mannville, Nordegg, Belloy/Debolt, Wabamun, Ireton, Z-marker and reefal Leduc events are interpreted in the median filtered $\mathbf{Z_{up}(+TT)}$ data and shown in panel 5 of Figure 6.6.

6.4.2 Near offset VSP deconvolution

Multiple reflections are represented in the downgoing wavefield as shown in panel 3 of Figure 6.6. The initial downgoing pulse (except in the case of head wave contamination) is the primary downgoing P-wave; later downgoing arrivals are multiples. The deconvolution IPP was designed as shown in Figure 6.7 to enable the monitoring of the deconvolution process.

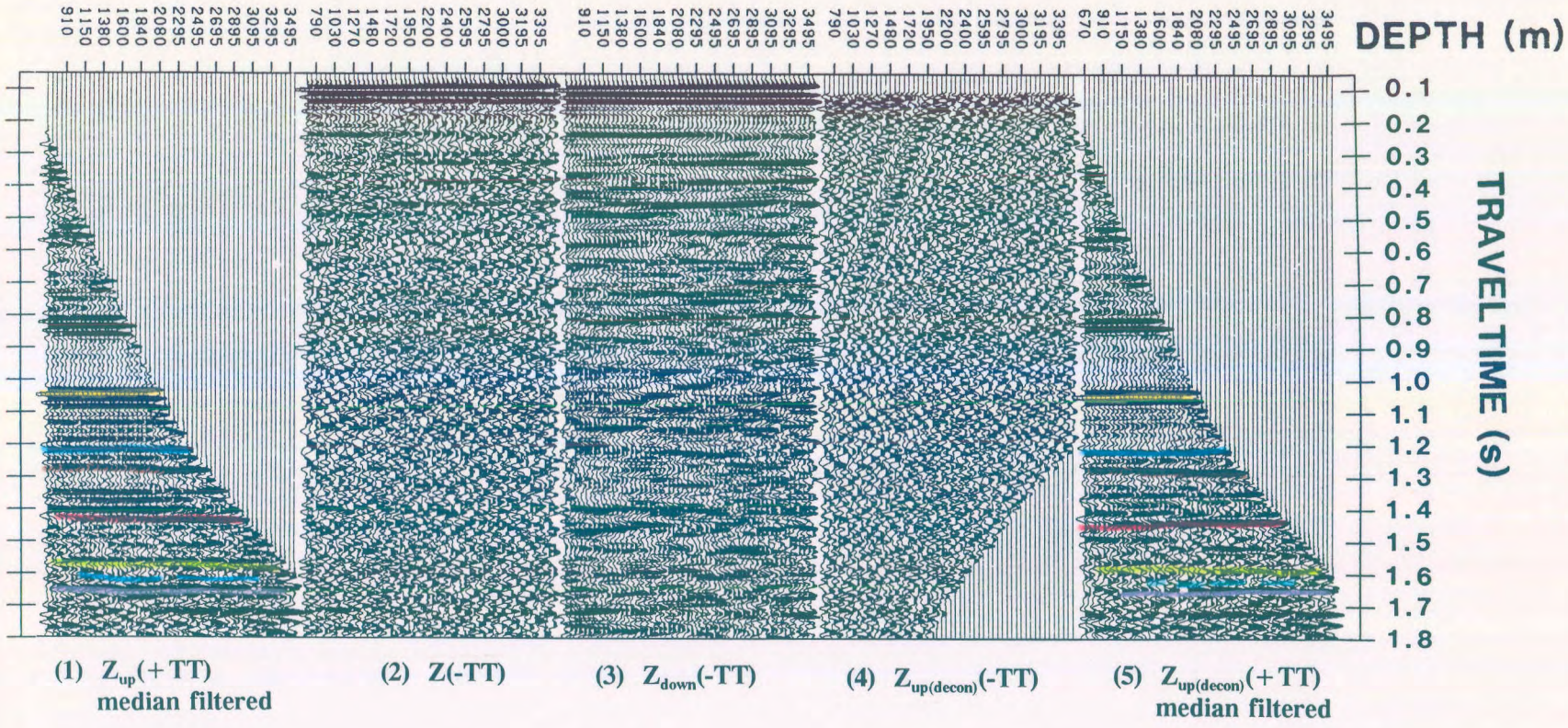

Figure 6.7 Interpretive processing panel depicting the deconvolution of the near (252 m) offset Simonette VSP data (from Hinds et al., 1993b and 1994c).

Panel 1 of Figure 6.7 is the median filtered $\mathbf{Z_{up}(+TT)}$ data. Panels 2, 3, and 4 are the $\mathbf{Z(-TT)}$, $\mathbf{Z_{down}(-TT)}$ and $\mathbf{Z_{up(decon)}(-TT)}$ data, respectively. The median filtered $\mathbf{Z_{up(decon)}(+TT)}$ data are displayed in panel 5.

A comparison of the $\mathbf{Z_{up}(+TT)}$ with $\mathbf{Z_{up(decon)}(+TT)}$ data, illustrates the effect of multiple contamination on the continuity of primary events. In panel 1 for example, the Debolt/Belloy event is high amplitude and continuous at sonde depths below the Mannville (from 2080 m to 2570 m). At shallower recording depths, the Debolt/Belloy event and a Mannville interbed multiple are interpreted to interfere. In more detail, the peak at 1.275 s on the left hand side of panel 1 is the interfering multiple. This event can be traced across the panel until the 2080 m trace. At that point, the Debolt/Belloy event peak (of lower frequency than the multiple) dominates and is continuous until the 2570 m trace; upon which it no longer exists since this is where the "first break" for that depth level now exists. On panel 5, deconvolution appears to have substantially reduced the effect of multiple interference as the Debolt event is much more continuous and the series of multiples immediately below the Mannville are strongly attenuated.

Within the zone from the Wabamun to Leduc Formation, multiple contamination is interpreted to be minimal since the events in this zone are continuous and unchanged after deconvolution. The Z-marker and Leduc events are continuous and do not exhibit either significant apparent time-structural relief or appreciable character variations. The description of the 524 m VSP interpretation will show that the far offset data do contain an interpreted multiple associated with the Wabamun interface in contrast to the near offset results presented above in which multiple generation at the Wabamun level is minimal.

6.4.3 Inside and outside corridor stacks

Multiple contamination on the $\mathbf{Z_{up}(+TT)}$ data can be re-examined using the inside and outside corridor stacks of both the $\mathbf{Z_{up}(+TT)}$ and $\mathbf{Z_{up(decon)}(+TT)}$ data.

$\mathbf{Z_{up}(+TT)}$ inside and outside corridor stacks along with the input data to the muting and stacking processes are shown in Figure 6.8. The amplitude of the Debolt/Belloy primary is weak on the $\mathbf{Z_{up}(+TT)}$ inside corridor stack shown in panel 4 of Figure 6.8 in comparison to the same event on the outside corridor stack as displayed in panel 3. The Debolt/Belloy event at sonde depths shallower than 2080 m (above the Mannville) on the muted input data shown in panel 5 for the $\mathbf{Z_{up}(+TT)}$ inside corridor stack is masked (destructively interfered with) by a possible interbed multiple. At depths greater than the Mannville (2080 m), the Debolt/Belloy event is unaffected by the multiple contamination, much higher in amplitude and 5-10 ms deeper in time therefore confirming that the bottom generating interface for this multiple is the Mannville Formation interface.

On the inside and outside $\mathbf{Z_{up(decon)}(+TT)}$ corridor stacks shown in Figure 6.9, the upgoing multiples appear to have been substantially attenuated by deconvolution. As an example, the Mannville associated multiples that lie immediately beneath the Mannville primary event on the $\mathbf{Z_{up(decon)}(+TT)}$ data are greatly attenuated with respect to the $\mathbf{Z_{up}(+TT)}$ data. This can be seen by comparing panel 1 of Figure 6.8 to panel 1 of Figure 6.9 in the time window of 1.35 to 1.5 s. In Figure 6.8, the time window is contaminated with multiple reflection events (coloured turquoise blue in panels 1 and 4) whereas in Figure 6.9, the same time window is relatively free of multiples. One multiple reflection event to note lies just above

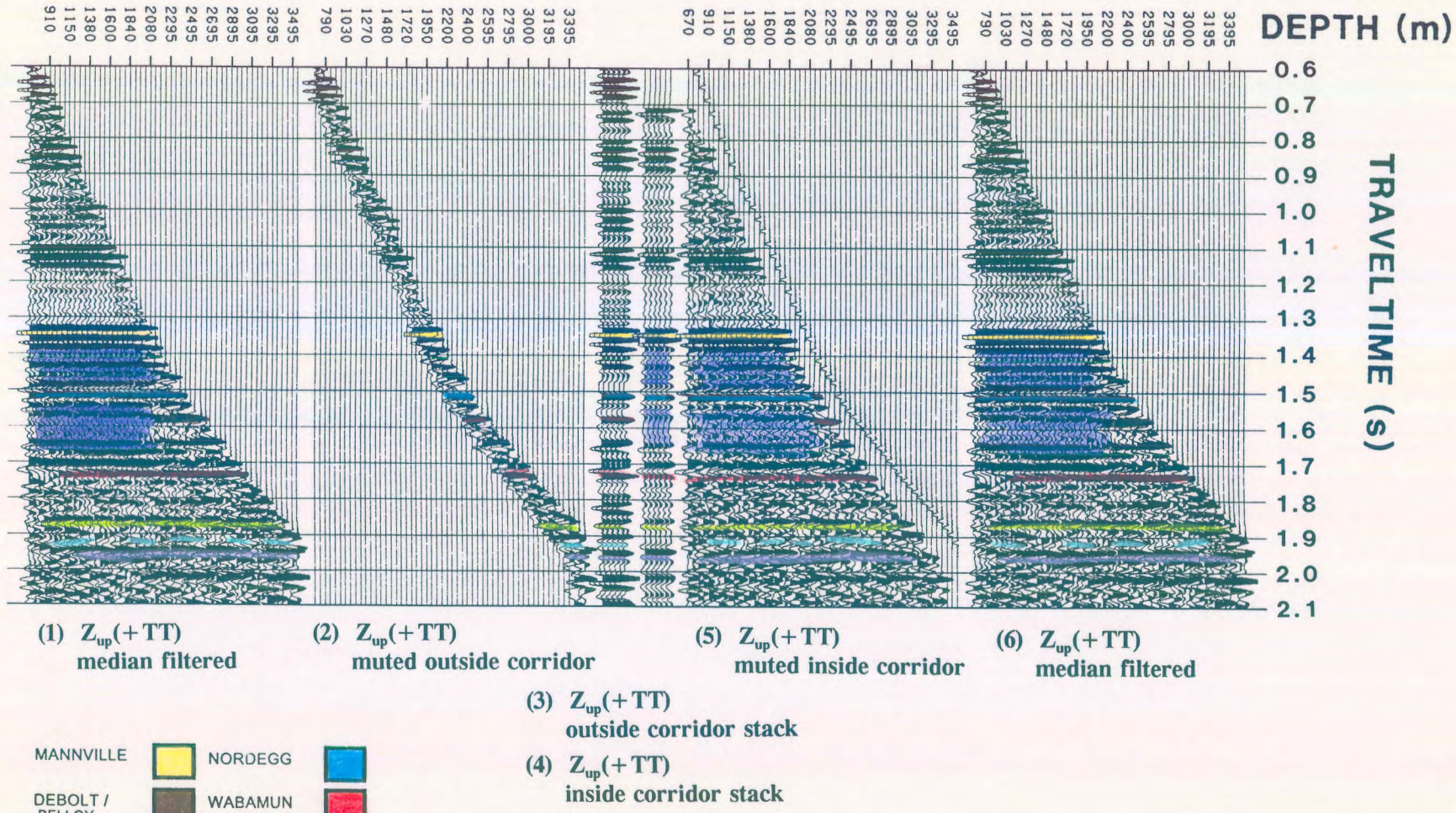

Figure 6.8 Interpretive processing panel illustrating the utility of the inside and outside corridor stacks of the near offset (252 m) Simonette $Z_{up}(+TT)$ data (from Hinds et al., 1993b and 1994c).

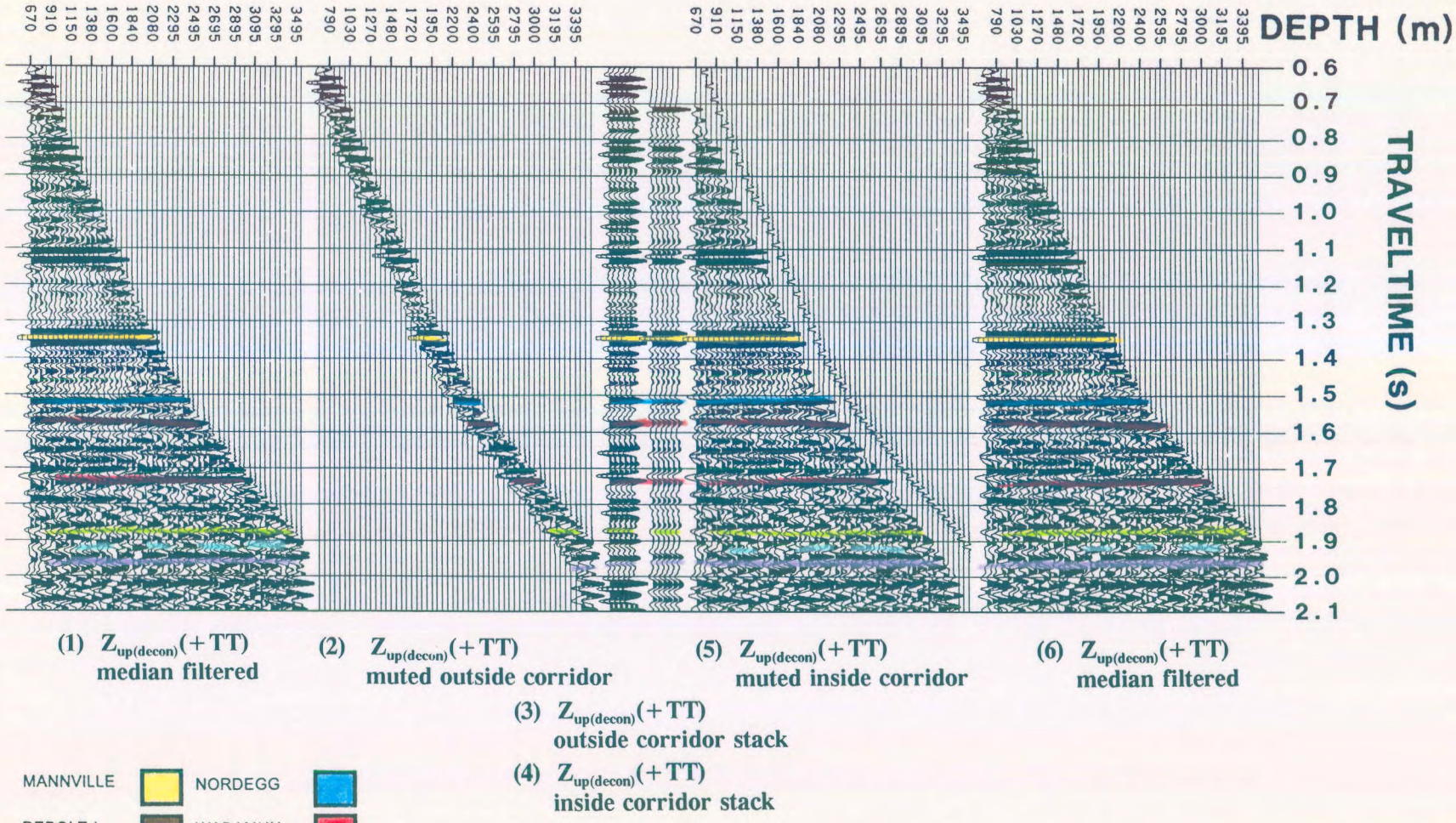

Figure 6.9 Interpretive processing panel illustrating the utility of the inside and outside corridor stacks of the near offset (252 m) Simonette $Z_{up(decon)}(+TT)$ data (from Hinds et al., 1993b and 1994c).

the Nordegg primary event at 1.48 s. On panel 1 of Figure 6.8, the event is dominant; however in panel 1 of Figure 6.9 (after deconvolution), the event is attenuated.

Some primary events recorded between the Mannville and Nordegg primary reflection events can only be seen on the few traces beyond the deepest trace recording the Mannville primary event. These few peaks will be included in the outside corridor stack. One such event is at 1.45 s which is preserved across the entire depth range of 670 to 2295 m once deconvolution is done. Since the depth interval between these primary events generated between the Mannville and Nordegg interfaces represents only a few traces, it causes the use of corridor stacks alone difficult to interpret without including the unmuted and muted corridor stack data on the same IPP (Hinds et al., 1989a).

6.5 Interpretive processing of the far offset VSP data

During the production consulting in 1987, the triaxial processing was not performed whilst the rig was on standby. The VSP-CDP mapped data recorded in 1987 used the $\mathbf{Z_{up}(+TT)}$ from the 524 m offset without the assistance of polarization analysis. The processing (Hinds et al., 1993b and 1994c) presented in this chapter is more extensive. The **Z(FRT)**, **X(FRT)** and **Y(FRT)** data contain nonpartitioned elements of the up- and downgoing P- and SV-wavefields. Hodogram-based rotation and time variant polarization rotation IPP's used in the processing of the far offset for the Simonette 524 m offset data (Hinds et al., 1989a; Hinds et al., 1991b; Hinds et al., 1993b and 1994c) are presented below to reveal that wavefield partitioning has significant implications for the interpretation.

6.5.1 Hodogram based rotation

The **Z(FRT)**, **X(FRT)**, and **Y(FRT)** data are presented in Figure 6.10 as panels 1, 2, and 3, respectively. The hodogram-based method initially polarized the components of the **X(FRT)** and **Y(FRT)** data outputting the **HMIN(FRT)** and **HMAX(FRT)** data (Hinds et al., 1989a; Hinds et al., 1993b and 1994c) shown in panels 4 and 5, respectively. **HMAX(FRT)** data display consistent primary downgoing P-wave first breaks indicating that the first set of rotations was relatively successful. The **HMAX(FRT)** data also contains mode-converted SV events (colored purple) that originate in the region of the Mannville reflector.

The **Z(FRT)** and **HMAX(FRT)** data were input to the second rotation which polarized the downgoing P-waves. Since the source offset distance is 524 m and the depth of the well is 3270 m, the **HMAX'** and **Z'** polarization axis were near vertical and horizontal, respectively. The resultant **Z'(FRT)** and **HMAX'(FRT)** data are shown in panels 6 and 7, respectively. The downgoing P-wave events are resident on the **HMAX'(FRT)** data; however, both the **HMAX'(FRT)** and **Z'(FRT)** data contain upgoing P-wave events. This indicates that the data will need to undergo time-variant polarization to separate the upgoing P-wave events onto a single data panel ($\mathbf{Z''_{up}}$) before interpretation.

The **Z'(FRT)** data (panel 6) contains the mode-converted downgoing shear wave primaries and possible multiples. In more detail, the first break on the 2080 m trace (representing the depth of the Mannville) can be approximated to be at 0.68 s on panel 6. At that point, the mode-converted downgoing SV event with a greater slope than the downgoing P-wave (the shallowest event coloured purple) can be traced down to 1.12 s on the 3570 m trace. Two

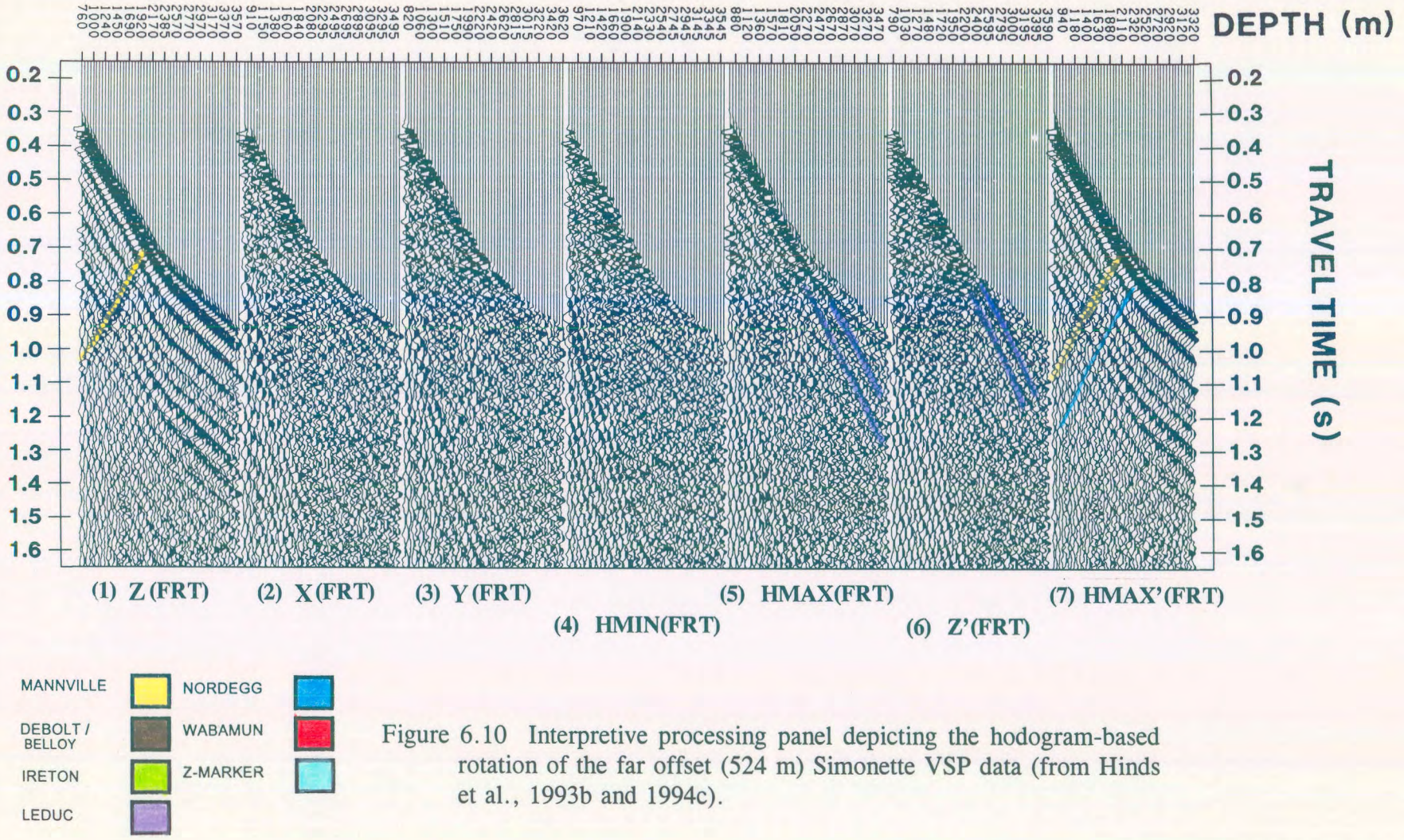

Figure 6.10 Interpretive processing panel depicting the hodogram-based rotation of the far offset (524 m) Simonette VSP data (from Hinds et al., 1993b and 1994c).

visible, downgoing SV-multiples (also coloured purple but arriving later in time than the primary downgoing SV primary event) parallel the primary and arrive within a 150 ms window on the 3570 m trace.

6.5.2 Time-variant model-based rotation

In the first stage of the time-variant model-based rotation, **Z'(FRT)** and **HMAX'(FRT)** data were wavefield separated (using F-K filtering; see chapter 2 for examples) into **HMAX'$_{down}$(FRT)**, **HMAX'$_{up}$(FRT)**, **Z'$_{down}$(FRT)** and **Z'$_{up}$(FRT)** data. The **HMAX'$_{down}$(FRT)** is retained and used in the deconvolution of the **Z"$_{up}$(FRT)** data in the following section. The deconvolution of the polarized far offset VSP data was not done during the 1987 processing and interpretation clarity will result from the deconvolution results shown below.

The **HMAX'$_{up}$(FRT)** and **Z'$_{up}$(FRT)** data shown as panels 1 and 2 in Fig. 6.11, respectively, were derotated (Hinds et al., 1989a) to output the **HMAX$_{up(derot)}$(FRT)** and **Z$_{up(derot)}$(FRT)** data shown in panels 3 and 4, respectively. Most of the upgoing P wave events have been distributed back onto the Z-type axis, **Z$_{up(derot)}$(FRT)**. In the **Z(FRT)** data shown in panel 1 of Fig. 6.10, the dominant downgoing P-waves were much higher in amplitude than the upgoing events resulting in the upgoing events being difficult to interpret. Following the wavefield separation, the separated upgoing P wave events in the **Z$_{up(derot)}$(FRT)** data are easily traceable within the data.

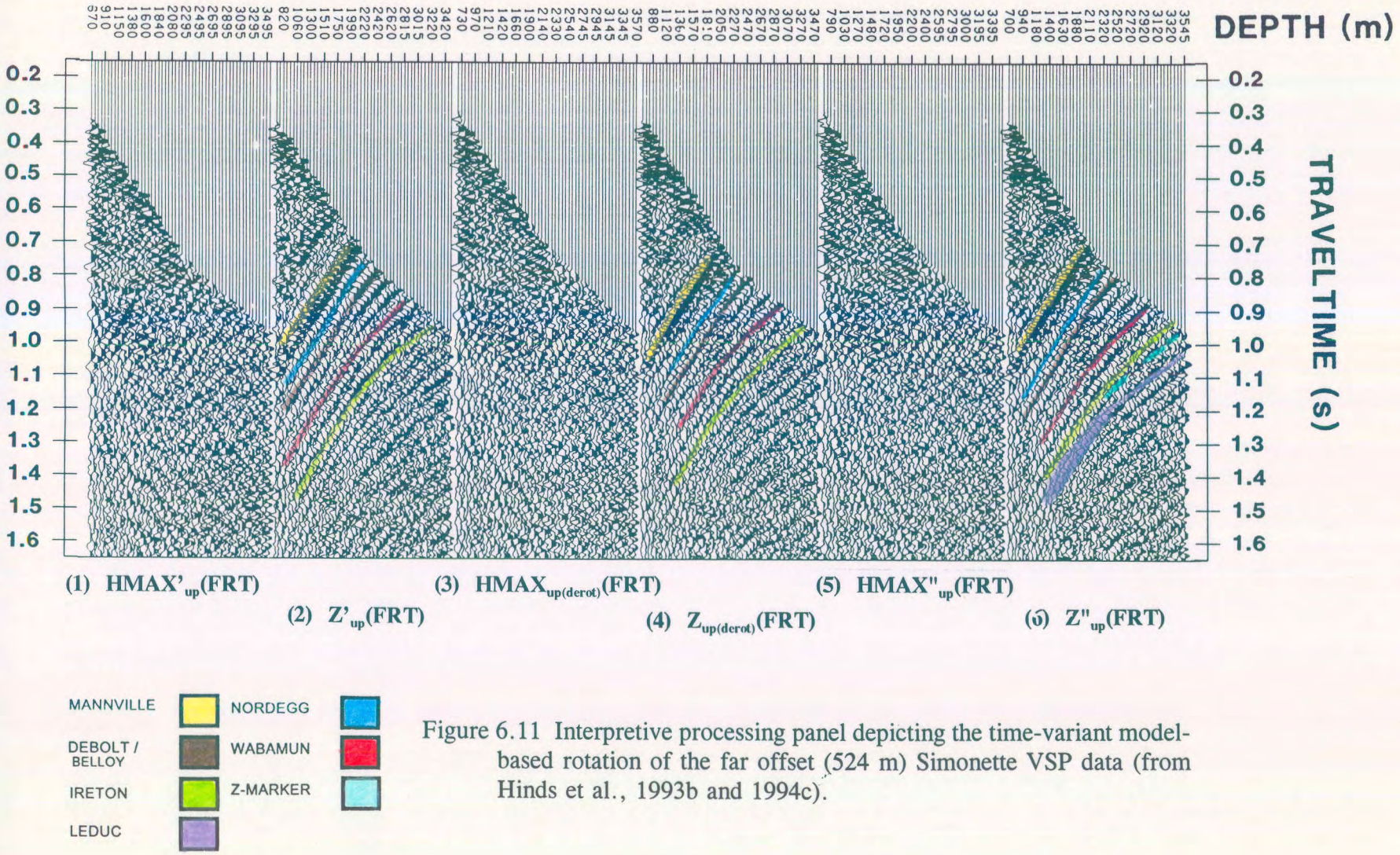

Figure 6.11 Interpretive processing panel depicting the time-variant model-based rotation of the far offset (524 m) Simonette VSP data (from Hinds et al., 1993b and 1994c).

The upgoing P-wave events on the $\mathbf{Z_{up(derot)}(FRT)}$ data shown in panel 4 are improperly aligned, particularly those generated by shallow reflectors, because of the choice of using a single rotation angle per data trace. These data have been derotated but the upgoing P-wave events are still partitioned on both output data sets, $\mathbf{Z_{up(derot)}(FRT)}$ and $\mathbf{HMAX_{up(derot)}(FRT)}$, due to the non-zero source offset.

To correct for misalignment, time-variant rotation angles were calculated (Hinds et al., 1991b; Hinds et al., 1993b and 1994c) and applied to every pair of traces in panels 3 and 4. The resultant $\mathbf{HMAX"_{up}(FRT)}$ data (panel 5) contains the residual downgoing SV-wave data left over in the data following wavefield separation. The $\mathbf{Z"_{up}(FRT)}$ data predominantly contains the upgoing P-wave events. On the $\mathbf{Z"_{up}(FRT)}$ data, shallow events (originating at 0.58 s between the traces for 1630 to 1750 m) are better isolated (onto a single panel) than on either the $\mathbf{Z_{up(derot)}(FRT)}$ data or $\mathbf{HMAX'_{up}(FRT)}$ data panels.

6.5.3 VSP-CDP mapping of the far offset VSP data

A VSP-CDP and migration IPP for the far offset $\mathbf{Z"_{up}(+TT)}$ and $\mathbf{Z"_{up(decon)}(+TT)}$ was designed to facilitate the interpretation of the interfering multiples and subsurface structure (Hinds et al., 1991b; Hinds et al., 1993b and 1994c). The $\mathbf{Z"_{up}(+TT)}$ data shown in Figure 6.12 were used for the interpretation of the low-relief Leduc reef. The appearance of many anomalous events arising from multiple contamination on the $\mathbf{Z"_{up}(+TT)}$ data (such as the event at 1.8 s) makes the interpretation of this plot along with the VSP-CDP (panel 3) and Kirchhoff migrated $\mathbf{Z"_{up}(+TT)}$ data difficult.

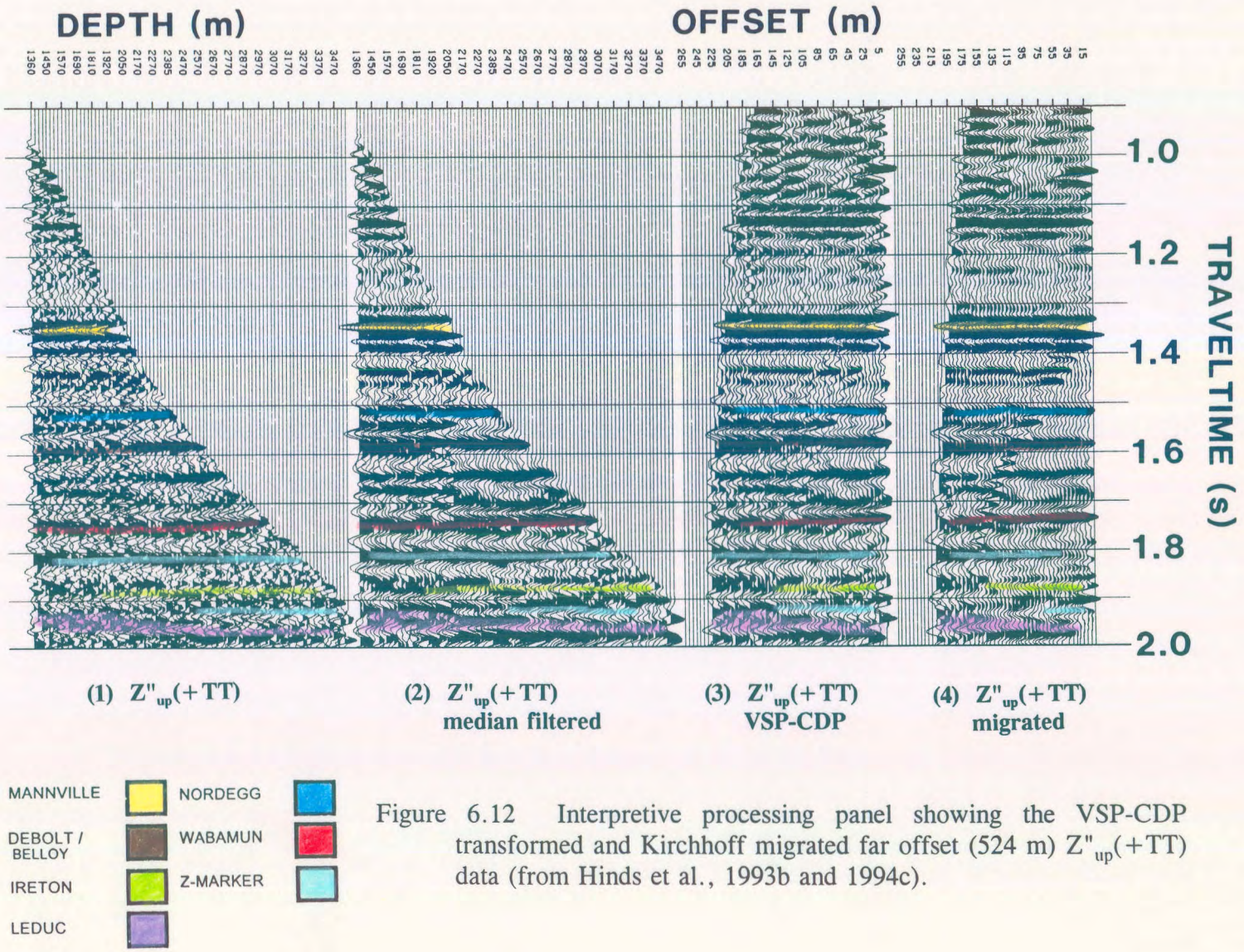

Figure 6.12 Interpretive processing panel showing the VSP-CDP transformed and Kirchhoff migrated far offset (524 m) $Z''_{up}(+TT)$ data (from Hinds et al., 1993b and 1994c).

The interpretation of the Leduc reef event is that the reef slope rises at 145 m away from the well; however the multiple events may be influencing the interpretation through destructive and constructive interference at the Leduc level.

Because of the relatively small offset of the source (524 m) in comparison to the overall depth of the borehole, far offset VSP deconvolution was attempted on the $\mathbf{Z''_{up}(+TT)}$ data as was shown in chapter 2. Nonmedian filtered $\mathbf{Z''_{up(decon)}(+TT)}$, median filtered $\mathbf{Z''_{up(decon)}(+TT)}$, VSP-CDP mapped (Dillon and Thomson, 1984) $\mathbf{Z''_{up(decon)}(+TT)}$ and Kirchhoff migrated $\mathbf{Z''_{up(decon)}(+TT)}$ data are shown, respectively, in panels 1-4 of Figure 6.13.

Two different sets of upgoing P-wave multiples are prevalent in Figure 6.12. One set of multiples are associated with the Mannville event. The nondeconvolved VSP-CDP and migrated data (Fig. 6.12) show Mannville (possibly interbed) multiples interfering with deeper P-wave primaries between 1.4 and 1.7 s. (specifically, 1.43, 1.56 and 1.68 s). Significant multiple contamination is interpreted between the shallowest trace and the 2080 m trace (top Mannville). Three multiple reflections are evident (coloured purple); the first Mannville multiple can be seen at 1.45 s, the second at 1.56 s (in between the Nordegg and Debolt primaries) and the third at 1.68 s.

The second set of multiples proved to be the most troublesome with respect to the reef interpretation during the initial processing done in 1987. There is a strong event (coloured light blue) below the Wabamun in the $\mathbf{Z''_{up}(+TT)}$ data at 1.8 s. It exists on the shallow traces down to the Wabamun and then abruptly disappears on the deeper traces from the

Wabamun reflector to total depth of the borehole. Was the interpretation of the reef events affected by this multiple event if the next occurrence of this Wabamun multiple existed? The interpreted reef flank shown in Figure 6.12 begins to rise around 145 m away from the borehole at 1.95 s up to 1.92 s. On the depth and time plots, the rise does not corresponds with the truncation of the multiple seen above at 1.8 s. This gives confidence in the interpretation that the rise in the reef event is due to the imaging of the reef slope; however interpretive processing must be used when faced with this decision!

In Figure 6.13, deconvolution has severely attenuated the Mannville and Wabamun multiple. The Mannville associated multiple events at 1.45, 1.56 and 1.68 s are attenuated and the Wabamun associated multiple event at 1.8 s is reduced from a dominant event to low amplitudes remnants. The Mannville, Nordegg, Debolt/Belloy, Wabamun, Ireton, Z-marker and Leduc events can now be more confidently correlated. The Leduc event can be interpreted on both the VSP-CDP and Kirchhoff migrated displays of Figure 6.13 to verify the interpretation of the nondeconvolved VSP-CDP and migrated data in the panels of Figure 6.12. The Z-marker (Fig. 6.13) rises gradually away from the location of the 13-15 well. The Leduc, although less discernable, is interpreted to rise gradually away from the borehole (basal Leduc) and rise to reef top at about 120-145 m from the borehole. The reflection from the top of the reef visually merges with the Z-marker event.

These results were used to assist in the construction of the preferred Ireton to Leduc isochron map shown earlier in Figure 6.5 (Hinds et al., 1991b and Hinds et al., 1993b and 1994c).

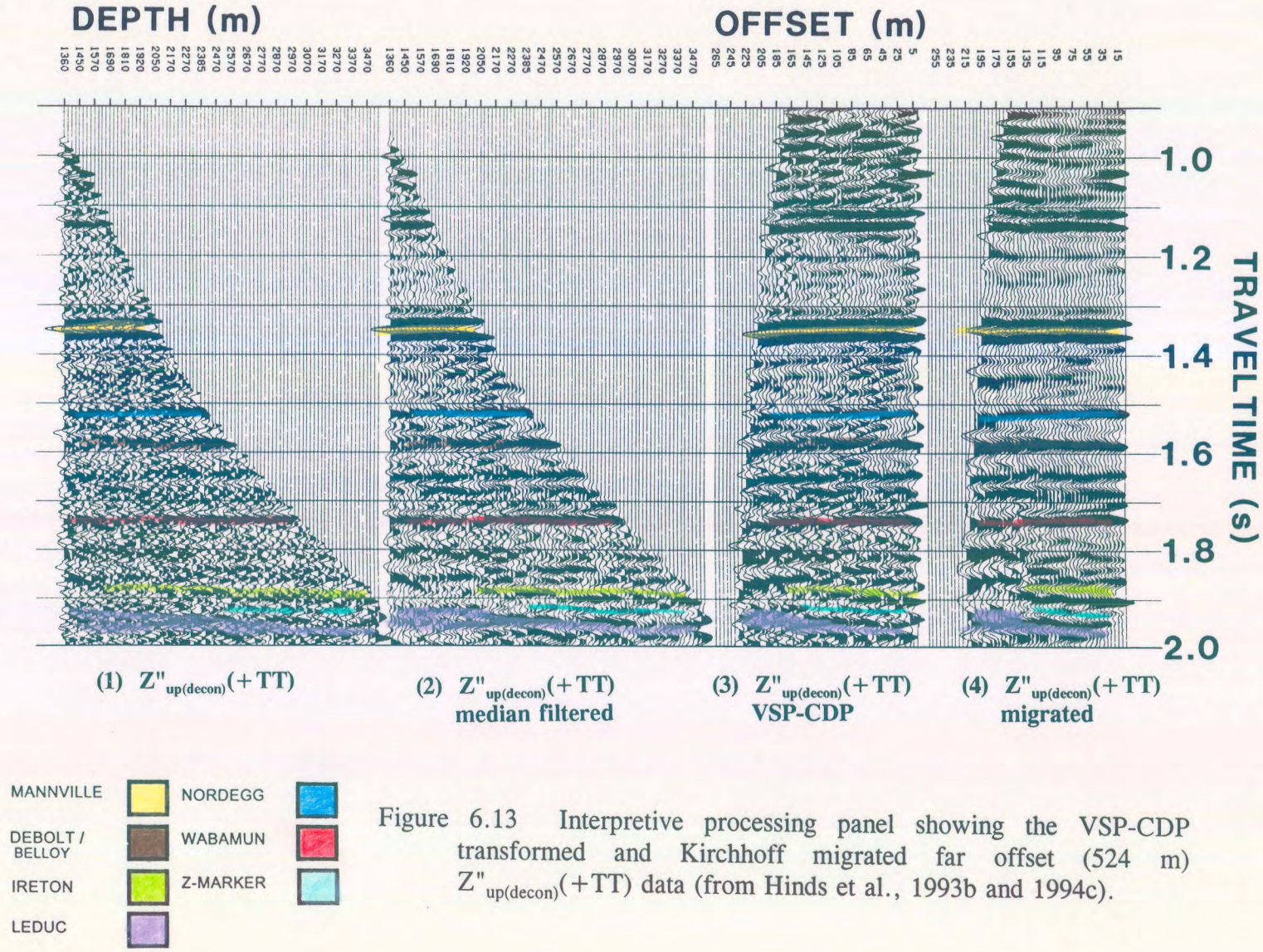

Figure 6.13 Interpretive processing panel showing the VSP-CDP transformed and Kirchhoff migrated far offset (524 m) $Z''_{up(decon)}(+TT)$ data (from Hinds et al., 1993b and 1994c).

6.6 Integrated interpretive display

On the left-hand side of the integrated interpretive display shown in Figure 6.14, sonic logs for wells 16-16 and 13-15, nondeconvolved, near offset, inside and outside corridor stacks are time-tied to the post-VSP interpretation of the surface seismic data. On the right-hand side, the $\mathbf{Z''_{up(decon)}(+TT)}$ data is time-tied to both the well 13-15 sonic log, and the deconvolved, near offset outside corridor stack. The horizontal (depth axis) of the $\mathbf{Z''_{up(decon)}(+TT)}$ data corresponds to the same scale used for the well 13-15 sonic and gamma ray log depth display.

The correlated data shown in Figure 6.14 allow for the confident interpretation of the surface seismic line and the identification of the Mannville, Nordegg, Debolt/Belloy, Wabamun, Ireton, Z-marker, and Leduc events. The Leduc event can be tied exactly at well 16-16 using the integrated sonic log from that well. The sloping reef event from well 16-16 to well 13-15 can be interpreted through the trough that gently slopes deeper in traveltime. Note that within the inter-reef shale interval, the sonic-log based synthetic seismogram is a poor fit to the VSP and surface seismic for the Ireton, Z-marker and Leduc events exhibiting up to a 5 ms tie. The sonic measurements could be at fault in that wellbore effects such as washouts, or the increased concentration of heavy drilling fluids injected into the borehole (intended to prevent a blowout) could have changed the sonic character of strata in the vicinity of the wellbore. Since the well was left open during the interpretation of the VSP survey data, it is reasonable to assume that the well engineers took precautionary steps to stabilize the fluids within the well. Alternatively, these misties could be related to wavelet variability or phase problems with the data (Hinds et al., 1993b). Whatever the source, such

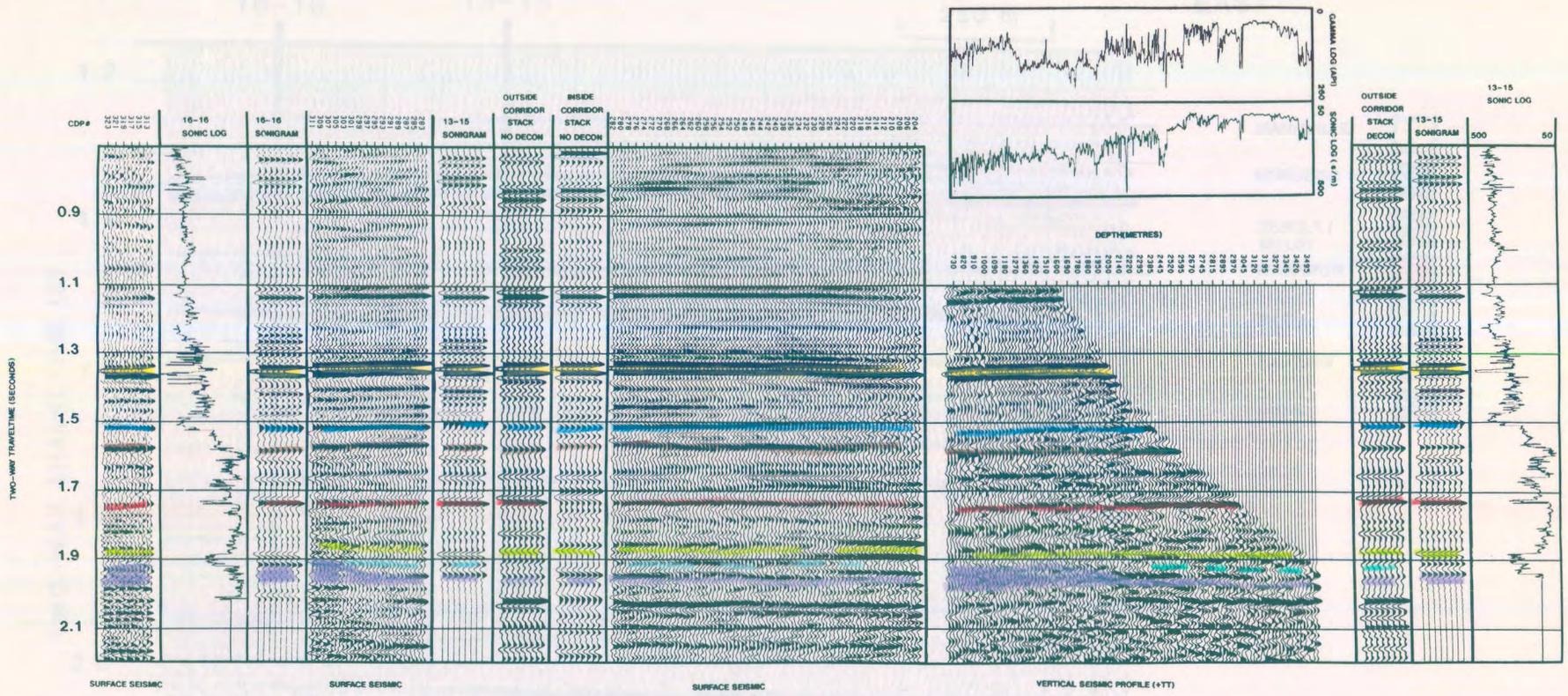

Figure 6.14 Integrated interpretive display showing the interpretation of the available exploration data for the Simonette reef case study (from Hinds et al., 1993b and 1994c).

discrepancies between sonic-log based synthetic seismograms and seismic data provide additional justification for acquiring seismic profile data.

The preferred version of the surface seismic section (shown as a normal polarity display in Fig. 6.15) differs slightly in several respects from the pre-well interpretation (Fig. 6.3). Of particular significance is that on the updated version, the Z-marker is present at the well 13-15 location, indicating that the well is situated in a flank position. The reinterpretation of the seismic line exhibits a flat reef extending from the borehole out to 100-120 m from the borehole. This is in agreement with the interpreted near and far offset VSP data. Beyond the coverage of the VSP, the reef crests. With respect to lateral variations in the thickness of the inter-reef shale isochron values (shale thinning is indicative of reefal thickening) the following interpretations can be made:

1) the inter-reef shale isopach as derived from the VSP data is 136 m (isochron value of 63 ms) on the trace nearest the 13-15 well;
2) the shale is 120 m (55 ms) at distances on the order of 100 m laterally from the well; and
3) the shale is 102 m (47 ms) at traces representing a distance of around 150 m from the well.

On the basis of the reinterpreted surface seismic and VSP data, a revised inter-reef shale isochron map (incorporating available well and surface seismic data) was drafted (Fig. 6.5). The 13-15 exploratory well is shown to be in a reef flank position, and indicates that the crest of the low-relief reef is in excess of 150 m west of well 13-15.

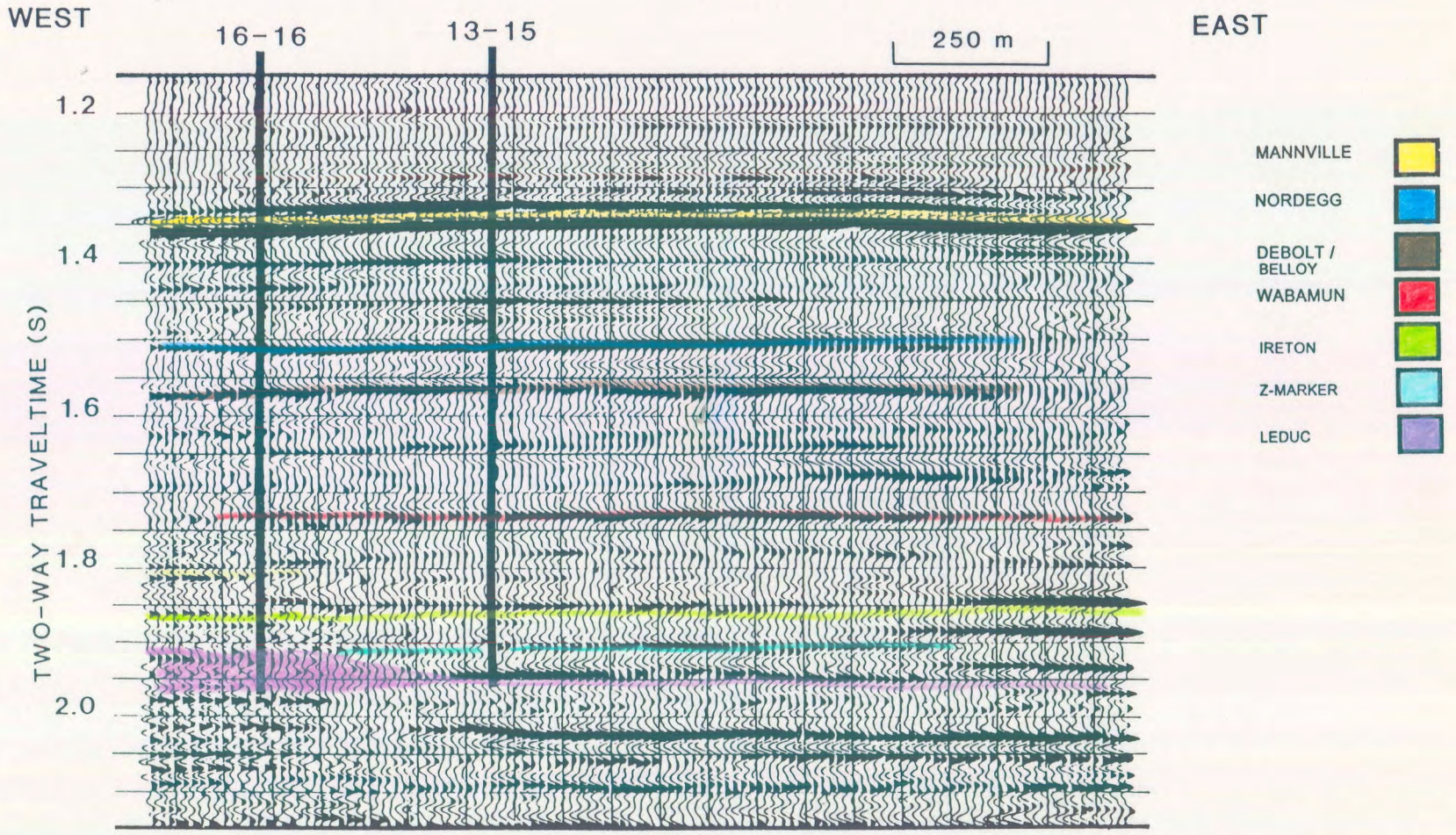

Figure 6.15. Current, preferred interpretation of the example seismic section. The Z-marker is laterally continuous at the 13-15 well location and the reef slope has been reinterpreted to be at least 150 m to the East of well 13-15 (from Hinds et al., 1993b and 1994c).

6.7 Conclusions

The 13-15-63-25 W5M exploratory well was drilled into low-relief Leduc reef in the Simonette area, Alberta. The well was prognosed to intersect the crest of the reef and to encounter about 50-60 m of pay. Unfortunately, according to the interpretation of all of the well data, it appears that the well was drilled into a flank position and ultimately abandoned. The decision to abandon the well, as opposed to whipstocking, was made after the acquisition and interpretive processing of the near and far offset VSP data, and after the reanalysis of existing surface seismic data. The VSP data were acquired and interpreted while the drill rig remained on-site, awaiting the decision to whipstock or abandon.

On the basis of VSP data the operator was able to: (1) determine an accurate tie between the surface seismic data (Fig. 6.15) and the subsurface geology, and identify a mistie between the surface seismic and sonic log seismogram; (2) determine that the reef was not close enough to well 13-15 to make whipstocking a viable option given the production penalties involved in drilling out of the target area; and (3) identify surface-generated and interbed multiples, and ascertain their effect on the surface seismic.

CHAPTER 7

SUMMARY AND CONCLUSIONS

The first two aims of this study were to:

(1) develop the methodology of Interpretive Processing (Hinds et al., 1989a) for VSP data using the interpretive processing panels (IPP), interactive data processing, integrated log display (ILD), integrated seismic display (ISD) and the integrated interpretation display (IID); and

(2) review the usage of the processing steps in the individual IPP to illustrate the incorporation of VSP interpretation to minimize processing artifacts (Hinds et al., 1994c).

A suggested processing runstream that was initially used in the VSP interpretive processing work of Hinds et al (1989a) was used as a starting point in the development of the interpretive processing displays. The major factors within VSP processing such as wavefield separation, near offset deconvolution, far offset data hodogram-based and time variant polarization, VSP-CDP transformation and migration were thoroughly discussed and used to illustrate the use of interpretive processing to locate, understand and correct for processing artifacts within the data processing sequences.

The interpretive processing panels were used to quality control processing routes (such as

wavefield separation shown in Flowcharts 1 through 6), link seismic data to geologic well log data (as in the ILD), merge VSP-CDP transform (or migration) results with surface seismic (as in the ISD) and to collect and merge all available exploration data into a single descriptive display (as in the IID). For the wavefield separation, the median filter (plus subtraction), K-L, F-K and τ-P based method were described with the emphasis being on the interpretation of possible processing artifacts inherent in the use of each method and their resolve. In the F-K based wavefield separation, batch processing and interactive F-K filtering were highlighted and the use of each was described through example data processing. Several different ways to use the same method to attack a particular "noise" problem such as multiple or tubewave contamination was shown for the F-K and τ-P based methods.

Multiple contamination and attenuation for both near and far offset data were shown through the use of the deconvolution IPP, inside and outside corridor stack IPP and the far offset deconvolution IPP. The final interpretation of the lateral extent of anomalies were shown thorough the use of the IPP's that included the VSP-CDP (migration) results. The concluding exploration picture was summarized through the use of the IID. In all of these displays for the various processing procedures, integrated geophysical/geological interpretation quality controlled and guided corrective or further processing.

The third and fourth aims were to:

(3) present the usage of VSP interpretive processing in four case studies, Lanaway Field (Hinds et al., 1989a; Hinds and Botha, 1989b; Hinds et al., 1994a and 1994c);

Ricinus Field (Hinds at al., 1989a; Hinds and Botha, 1989c; Hinds et al., 1993c; Hinds et al., 1994c), Fort. St. John Graben (Hinds et al., 1991a, Hinds et al., 1993a; Hinds et al., 1994b; Richards et al., 1994; Hinds et al., 1994c) and Simonette Field (Hinds et al., 1991b; Hinds et al., 1993b and 1994c); and

(4) further the method of integrated geophysical/geological interpretation (Anderson, 1986) using the case studies.

In the Lanaway Field case study shown in Chapter 3 which deals with oil and gas exploration along the Rimbey-Leduc-Meadowbrook carbonate reef "chain" in Alberta, Canada, the original interpretation of the seismic data which indicated 80 m of possible anomalous accretionary reef growth led to the drilling of a well that penetrated oil and gas bearing reef that was similar to surrounding successful Leduc wells. By means of interpretive processing through the use of IPP's and IID, an updated interpretation was developed that was consistent with the geological log data. Multiple contamination was examined and three possible explanations for the anomalous seismic character and time-structural anomaly was stated. Of these three explanations, the presence of possible Winterburn patch reefing and the tuning effect on the seismic data caused by surrounding Ireton drape was put forth as most likely to be the cause of the seismic anomaly (Hinds et al., 1989a; Hinds and Botha, 1989b; Hinds et al., 1994a and 1994c). The final interpretation differed from the original as the correct seismic placement of the Leduc reef at the well location was found.

In the Ricinus Field case study shown in Chapter 4 which deals with gas exploration in the Ricinus Leduc carbonate atoll reef in central Alberta, the original interpretation of the

seismic data which predicted the intersection of Leduc reef led to the drilling of a well that penetrated off-reef Woodbend Group shales. A near and far offset VSP surveys were run. Through the use of interpretive processing using near and far offset IPPs and ISD, the seismic was correlated to the geological logs. An updated geological model was developed and the final interpretation differed from the initial interpretation as the edge of the reef (in the direction of the far offset source location) on the seismic section was postulated to at least 500 m away from the well.

In the Fort St. John Graben case study shown in Chapter 5 which deals with channel sand gas accumulations in Lower Carboniferous strata, the original interpretation predicted the intersection of gas bearing basal Kiskatinaw sandstones and the presence of a single fault between the VSP well and well 2-25 to the North. The interpretation led to the drilling of a basal Kiskatinaw sandstone with a high shale content which was non-commercial. A near offset and two far offset VSP surveys were run. The interpretive processing of the near offset VSP data led to an updated seismic correlation to the geology at the well in addition to the revealing of extensive multiple contamination. The interpretive processing of the far offset VSP data (FSJG1) which imaged the subsurface towards the seismic line (and the VSP well) led to the interpretation of a lateral character anomaly within the basal Kiskatinaw event (which could be caused by increased shale content) and the location of two faults throughout lower and upper Carboniferous strata which were unresolved on the surface seismic (Hinds et al., 1993a and 1994b; Hinds et al., 1994c). The far offset VSP data (FSJG2) which imaged the subsurface to the East of the well (away from the seismic line and the VSP well) explored for basal Kiskatinaw channel sands and faulting. The interpretive processing showed a continuous basal Kiskatinaw and the imaging of two faults which are interpreted

to be related to the faulting seen on the other far offset VSP data. The updated interpretation differed from the original due to the accurate mapping of the lower and upper Kiskatinaw (which produced gas at the VSP well) in the vicinity of the VSP well and the detailing of faulting which was poorly imaged by the surface seismic.

In the Simonette Field case study shown in Chapter 6 which deals with oil exploration in the Simonette Reef in North-western Alberta, the original interpretation of the seismic data which prognosed the penetration of 50-60 m of productive carbonate reef led to the drilling of a well that penetrated off-reef shales. A near and far offset VSP were run whilst the drilling rig was on-site in order to determine if whipstocking the well towards a known producing well 16-16 (within the same reef) was viable. The interpretive processing of the near offset data determined an accurate correlation to the geological wells, identified possible multiple contamination and showed that the edge of the reef was not evident up to distance of 120 m from the VSP well. The interpretive processing of the far offset data showed possible Wabamun multiple contamination, confirmed the reef slope interpretation from the near offset VSP data, located the edge of the reef to be approximately 155 m from the VSP well and showed that the reef did not reach the buildup that was found in well 16-16 even at a distance of 195 m from the VSP well. The updated interpretation differed from the original interpretation in that detailed imaging of the reef slope and an accurate correlation to the geological well results were achieved. The integrated geophysical/geological interpretation resulted in the decision that it was not economically feasible to whipstock the VSP well.

In conclusion, it seems evident that interpretive processing resulted in a greater understanding of the processing of the VSP data by the merging of the interpretation and processing

procedures. The interpretive processing displays were used in the integrated geophysical/geological interpretations to further the knowledge about the subsurface in each of the case studies. The method of integrated geophysical/geological interpretation which previously primarily dealt with surface seismic and geological data has been further developed to include VSP data (Hinds et al., 1994c).